Research Paper

Mussel-inspired conductive nanofibrous membranes repair myocardial infarction by enhancing cardiac function and revascularization

Yutong He[#], Genlan Ye[#], Chen Song, Chuangkun Li, Weirong Xiong, Lei Yu, Xiaozhong Qiu[✉], Leyu Wang[✉]

Guangdong Provincial Key Laboratory of Construction and Detection in Tissue Engineering, Department of Anatomy, Southern Medical University, Guangdong, Guangzhou 510515, China.

# These authors contributed equally to this work.

✉ Corresponding authors: Prof. Leyu Wang, Guangdong Provincial Key Laboratory of Construction and Detection in Tissue Engineering, Department of Anatomy, Southern Medical University, Guangdong, Guangzhou 510515, China. Email: wangleyu889@163.com Telephone: 86-20-61647752. Prof. Xiaozhong Qiu, Guangdong Provincial Key Laboratory of Construction and Detection in Tissue Engineering, Department of Anatomy, Southern Medical University,Guangdong, Guangzhou 510515, China. Email: qqiuxzh@163.com Telephone: 86-20-61648401

Abstract

The controversy between polypyrrole's (Ppy) biocompatibility and its aggregation on nanofibers impedes application of conductive Ppy-incorporated nanofibers to create engineered cardiac microenvironments. The purpose of this study was to fabricate a functional scaffold for engineering cardiac patches (ECP) using a high concentration of methyl acrylic anhydride-gelatin (GelMA)-Ppy nanoparticles, mussel-inspired crosslinker, and electrospun (ES)-GelMA/polycaprolactone (PCL) nanofibrous membrane.

Methods: First, spherical GelMA-Ppy nanoparticles were obtained when the methacrylate groups of GelMA formed a self-crosslinked network through oxidative polymerization of Ppy. Second, GelMA-Ppy nanoparticles were uniformly crosslinked on the ES-GelMA/PCL membrane through mussel-inspired dopamine-N'N'-methylene-bis-acrylamide (dopamine-MBA) crosslinker. Finally, the feasibility of the dopa-based conductive functional ECP scaffold was investigated *in vitro* and *in vivo*.

Results: The GelMA-Ppy nanoparticles displayed excellent biocompatibility at a high concentration of 50 mg/mL. The massive GelMA-Ppy nanoparticles could be uniformly distributed on the ES nanofibers through dopamine-MBA crosslinker without obvious aggregation. The high concentration of GelMA-Ppy nanoparticles produced high conductivity of the dopamine-based (dopa-based) conductive membrane, which enhanced the function of cardiomyocytes (CMs) and yielded their synchronous contraction. GelMA-Ppy nanoparticles could also modify the topography of the pristine ES-GelMA/PCL membrane to promote vascularization *in vitro*. Following transplantation of the conductive membrane-derived ECP on the infarcted heart for 4 weeks, the infarct area was decreased by about 50%, the left ventricular shortening fraction percent (LVFS%) was increased by about 20%, and the neovascular density in the infarct area was significantly increased by about 9 times compared with that in the MI group.

Conclusion: Our study reported a facile and effective approach to developing a functional ECP that was based on a mussel-inspired conductive nanofibrous membrane. This functional ECP could repair infarct myocardium through enhancing cardiac function and revascularization.

Key words: dopamine, polypyrrole nanoparticles, electrospun membrane, myocardial infarction, revascularization

Introduction

Engineered cardiac patches (ECP), which consist of seeding cells and scaffolds, provide promising strategies for infarcted myocardium regeneration [1-3]. Biomimetic microenvironments consisting of

ECP can promote cardiomyocyte (CM) function and yield synchronous contraction *in vitro* [4-7]. They can also repair myocardial infarction and enhance cardiac function *in vivo* [6, 8]. ECP relies on the composite or natural matrix materials (the scaffolds) to retain a mass of therapeutic cells (CMs or cardiac progenitor cells) in proximity to the infarct myocardium, and repair myocardial infarction through a possible paracrine mechanism [9-11]. Thus, scaffolds have a pivotal role in ECP construction. For the construction of functional ECP, many conventional as well as modified techniques have been used to develop biomimetic scaffolds, such as 3-dimensionally printed scaffolds, macroporous hydrogel, and electrospun (ES) fibers [12-15]. Among these, ES is a well-developed technique with the advantages of cost-efficiency, easy operation, and versatility. ES fibers are widely used in ECP scaffolds due to their unique characteristics, including high surface area to volume ratios for cell growth and retention and tunable fiber diameters to mimic the fibrous topography of myocardium microenvironment [16-18].
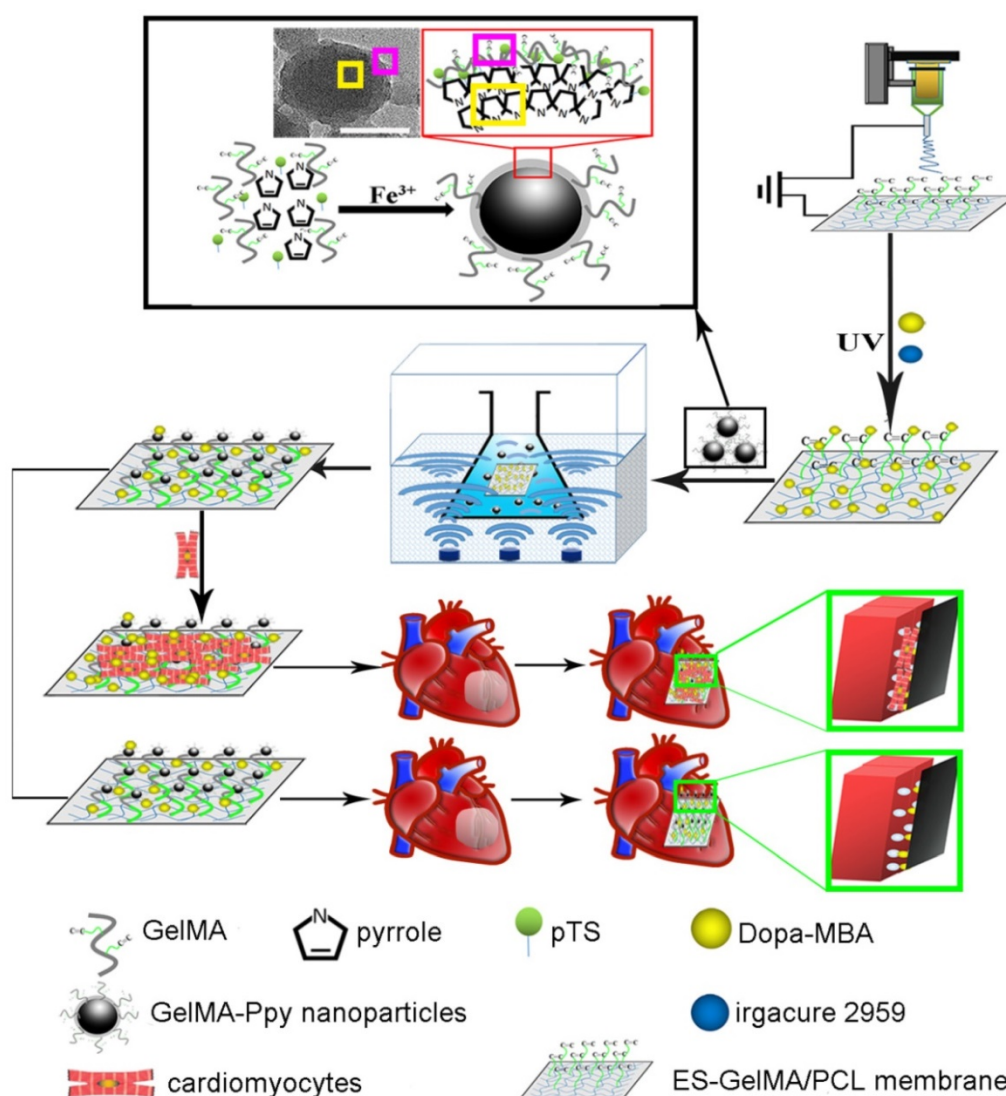
As is well known, conductivity performance is essential to sustain the cardiac physiologic function. The high conductivity of myocardium can efficiently transmit electrical signals intra- and inter-cardiac cells, which is indispensable for electric contraction coupling and synchronous contraction of the whole heart [19-21]. Conductive polymers, such as polypyrrole (Ppy) and polyaniline, have been employed in ES-produced ECP scaffolds because of their high conductivity and good electrical stability [22-26]. However, generation of highly conductive and biocompatible fibers using a high concentration of conductive polymers is still a significant challenge. Fabrication of ES fibers from pristine conductive polymers is expensive and difficult due to the limitation of suitable solvents for conductive polymer dissolution [27]. The blending of conductive and biodegradable polymers for making ES is a commonly-used method to generate conductive fibers. However, the concentration of conductive polymer must be very low for its uniform distribution in fibers [28], and the appropriate ratio of conductive polymer to biodegradable polymer should be further explored to avoid aggregation of the conductive polymer on the surface of fibers [29].

Direct deposition of conductive polymer on as-spun fibers is a reported alternative method. During oxidative polymerization of Ppy, it is simultaneously distributed on the fibers to produce the conductive scaffold [29, 30]; however, the introduction of an oxidizing agent would have potential cytotoxicity and Ppy easily aggregated on the fibers during this process. Our previous study demonstrated that the crosslinker dopamine-N'N'-methylene-bis-acrylamide (dopa-MBA) could incorporate Ppy into a methyl acrylic anhydride (MA)-gelatin (GelMA)/poly (ethylene glycol) diacrylate (PEGDA) cryogel, which displayed good biocompatibility and high conductivity [31]. Dopamine, inspired by mussel adhesive protein, generated interest in the regenerative medicine field due to its excellent adhesive and crosslinking function [32-36]. When dopamine reacts with MBA through Michael addition reaction to form a double-bond crosslinker, this mussel-inspired crosslinker could quickly graft onto the GelMA/polycaprolactone (GelMA/PCL) nanofibers by photoinitiators [37, 38].

In this study, dopamine-MBA-grafted (dopa-grafted) GelMA/PCL nanofibers were crosslinked with GelMA-Ppy nanoparticles under concussive conditions (**Scheme 1**). We hypothesized that massive GelMA-Ppy nanoparticles could be uniformly distributed on the GelMA/PCL ES fibers by the dopamine-MBA crosslinker and substantial GelMA-Ppy nanoparticles would endow the fibers with high conductivity.

The biocompatibility of high concentrations of Ppy remains controversial, although biomaterials incorporated with high concentrations of Ppy have high conductivity [39-41]. Higher than 9.7 µg/mL Ppy polymerized by oxidative doping has been considered harmful for cell viability/proliferation [42]. A recent *in vitro* study reported that polypeptide-conjugated Ppy-coated metal electrode displays excellent cytocompatibility [43, 44]. Gelatin, a natural polymer, can be self-crosslinked into a monomolecular or network structure in dilute solutions [45-47]. In this study, as shown in **Scheme 1**, GelMA was used as a shape-inducer and a toxicity-neutralizer to form the GelMA-Ppy nanoparticles during the process of oxidative polymerization. The excellent biocompatibility of GelMA-Ppy nanoparticles was still sustained even at high concentration (50 mg/mL). Accordingly, a mussel-inspired conductive membrane was developed through crosslinking the dopa-grafted GelMA/PCL nanofibers and massive GelMA-Ppy nanoparticles. This mussel-inspired conductive membrane, which possesses good biocompatibility and high conductivity, promoted CMs function and angiogenesis *in vitro* and holds promise to repair myocardial infarction by enhancing cardiac function and revascularization.

Scheme 1. Schematic illustration of the fabrication of mussel-inspired conductive membrane and its application in engineered cardiac tissue patch (ECP) in a rat MI model. During the oxypolymerization of Ppy, paratoluenesulfonic acid (pTS) served as the dopant, FeCl$_3$ acted as the oxidizing agent, and GelMA self-crosslinked onto the network structure, forming GelMA-Ppy nanoparticles. After the dopa-grafted ES-GelMA/PCL membrane was fabricated under the photoinitiator irgacure 2959, GelMA-Ppy nanoparticles were concussively crosslinked onto the dopa-MAB-grafted ES-GelMA/PCL membrane through the mussel-inspired dopamine crosslinker. Scale bar, 50 nm.

Methods

Materials

Poly (ε-caprolactone) (PCL) and gelatin were purchased from Sigma (St Louis, USA). Methanol, chloroform and alcohol were obtained from Macklin Chemical Reagent Company (Shanghai, China). Live/dead cell staining kit, Alexa Fluor 568 donkey anti-rabbit IgG (H&L), and Alexa Fluor 488 donkey anti-mouse IgG (H&L) were from Molecular Probes (Life Technologies). Cell Counting Kit-8 (CCK-8) was purchased from Dojindo Molecular Technologies (Japan). The primary antibodies of Ki67, α-actinin, connexin 43 (CX-43), and von Willebrand Factor (vWF) were acquired from Abcam. F4/80 antibody was purchased from Ebioscience (USA). Cell Navigator F-Actin Labeling Kit was from AAT

Bioques. Alpha smooth muscle actin (α-SMA) was ordered from Boster Biological Technology (Wuhan, China).

Preparation of GelMA

GelMA was prepared as described previously [31]. Briefly, 1 g gelatin was dissolved in 10 mL PBS buffer (0.01 M) that was maintained at 50 ℃ and then 0.5 mL methacrylic anhydride (MA) was added dropwise to the gelatin solution and stirred at 50 ℃ for 1 h. The reaction was terminated by adding 10 mL PBS. GelMA was obtained through dialysis and lyophilization.

Synthesis of GelMA-Ppy nanoparticles

500 mg GelMA was dissolved in 100 mL deionized water at 50 ℃ to form GelMA solution. Subsequently, 1417.65 mg of p-toluene sulfonic acid

was added to the GelMA solution and stirred for 3 h. Next, 500 mg pyrrole was added and stirred for 2 h. After solubilization, 1211.19 mg $FeCl_3$ was added to the solution and stirred overnight. The products were precipitated with an excess of ethanol. The pellets were washed three times with deionized water and dried under mild conditions (room temperature, and atmospheric pressure) to obtain GelMA-Ppy nanoparticles.

Preparation of dopamine-MBA crosslinker

Dopamine-MBA crosslinker was prepared according to a previously reported method [31, 48]. Briefly, water/ethanol (4:3 v/v) solution was adjusted to pH 6 using 5 M HCl. In 49 mL water/ethanol solution, 3500 mg MBA was added to the final concentration of 70.1 mg/mL. After solubilization, 3325 mg dopamine was added to the solution under nitrogen protection to exclude oxygen. The reaction was performed in an oil bath at 45 ℃ for 3 days in the dark. The dopamine-MBA crosslinker was obtained after lyophilization and stored at -20 ℃.

Fabrication of pristine ES-GelMA/PCL membrane

Pristine ES-GelMA/PCL membrane was obtained by the following procedure. 0.2 g GelMA and 0.2 g PCL were separately dissolved in 2.5 mL trifluoroethanol. After solubilization, the two solutions were mixed and stirred overnight. The GelMA/PCL mixture solution was loaded into a plastic syringe fitted with a 21 G metal spinneret, which was connected to a high voltage (18 kV) power supply (SS-UC, Bejing Ucalery Technology Development Company) for electrospinning. The distance from the needle to the aluminum foil was 16 cm and the flow rate was kept at 2 mL/h using a syringe pump. For the directly blending-spun ES-Ppy membrane, 250 mg GelMA-Ppy nanoparticles (final concentration 50 mg/mL) were added to the GelMA/PCL mixture solution and stirred overnight. Finally, the GelMA-Ppy-incorporated GelMA/PCL mixture solution was directly blending-spun to fabricate ES-Ppy membrane.

Preparation of mussel-inspired conductive membranes

A 2 cm × 2 cm ES membrane was dipped into 4 mL solution containing 5 mg/mL dopa-MBA and 1% irgacure 2959 (w/v) and reacted for 0.5 h under UV light. The dopa-grafted ES membrane was washed three times with deionized water and then dried at room temperature. The dopa-grafted ES membrane was immersed into 2 mL the GelMA-Ppy solution at the concentrations of 10, 20, or 50 mg/mL and then was subjected to an ultrasonic concussion for 2 h. After the reaction was completed, the samples were washed three times with deionized water and then dried at room temperature. Using this method, three dopa-based membranes, ES-P10, ES-P20, and ES-P50, were prepared. ES-P10, ES-P20, and ES-P50 membranes were dopa-grafted ES-GelMA/PCL membranes crosslinked with 10, 20, and 50 mg/mL GelMA-Ppy, respectively.

Characterization of GelMA-Ppy nanoparticles

The molecular structure of GelMA-PPy solid powder was analyzed by X-ray diffraction (XRD). A high-resolution Empyrean diffractometer (PANalytical) equipped with a CuKα1 X-ray source was used and operated at 40 kV. 2θ scans were recorded at angles ranging from 5° to 80° (2θ) in a continuous scan mode. The morphology of the GelMA-Ppy nanoparticles was observed under transmission electron microscopy (TEM; JSM-2010HR, Japan) at an acceleration voltage of 200 kV. The size distributions of GelMA-Ppy particles were detected using dynamic light scattering (DLS; Zetasizer Nano-Zs, Malvern Instruments, UK).

Characterization of conductive membranes

Contact angles were measured by placing liquid drops on samples for 20 s under a contact angle microscope (CAM, SOLON, USA) using configuration software (version 2.1.1). The electrical conductivity of the membrane was measured using a digital four-point probe (Suzhou Jingge Electronic Co. LTD, China). The ultrastructure of the conductive membrane was observed using scanning electron microscopy (SEM, S-3000N, Hitachi, Japan).

Cell culture

All institutional and national guidelines for the care and use of laboratory animals were followed. All procedures were approved by Southern Medical University Animal Ethics Committee. Primary cultured CMs were isolated from the hearts of 3-day-old Sprague-Dawley rats according to an established method [31]. Briefly, hearts were carefully dissected and dissociated into single-cell suspensions with 0.1% collagenase type II (Sigma). The suspended cells were centrifugated at 990 g for 5 min, and the harvested cells were pre-plated to separate CMs from cardiac fibroblasts for 2 h. The unattached CMs were collected and centrifuged at 990 g for 5 min. CMs were resuspended and seeded onto the scaffolds ($5×10^4$ cells/cm²) or glass slides ($2×10^4$ cells/cm²). CMs and cardiac fibroblasts were cultured separately in high-glucose Dulbecco's modified Eagle's medium (DMEM, GIBCO), supplemented with 15% fetal

bovine serum (FBS, GIBCO), 100 U/mL penicillin, and 100 µg/mL streptomycin. Human umbilical vein endothelial cells (HUVECs) were purchased from the cell bank of Chinese Academy of Sciences (Shanghai). HUVECs were seeded onto scaffolds (2×10^4 cells/cm^2) and were cultured with RPMI Medium 1640 (GIBCO) supplemented with 10% FBS, 100 U/mL penicillin, and 100 µg/mL streptomycin. The cells were cultured in an incubator at 37 °C under 5% CO_2 and the medium was changed every 2 days.

Biocompatibility detection

The biocompatibility of GelMA-Ppy nanoparticles was tested using live/dead staining and CCK-8 assay. After CMs were cultured on glass slides for 1 day, the cells were treated with different concentrations of GelMA-Ppy nanoparticles. At the indicated time, CMs were washed three times with PBS and stained with the live/dead working solution at 37 °C for 30 min in the dark. The images of the dyed samples were captured with a fluorescence microscope (Olympus, BX53, Japan). The survival ability of CMs cultured on the membrane was examined by live/dead staining with the above methods. The CCK-8 assay was performed as follows: CMs seeded onto different membranes were cultured in different wells in a 96-well culture plate, six wells per group. At the indicated time, the culture medium was replaced with 100 µL medium containing 10 µL CCK-8 solutions. After the samples were incubated in an incubator at 37 °C under 5% CO_2 for 2 h, 100 µL solution of each well was transferred into a second 96-well culture plate. The absorbance at 450 nm was measured using a microplate reader.

Immunofluorescence analysis

After culturing for 3 or 7 days, CMs on different membranes were fixed with 4% paraformaldehyde at 4 °C overnight. Cells were washed three times with PBS, permeabilized with 0.2% Triton X-100 in PBS at room temperature for 15 min, and blocked with 2% bovine serum albumin (BSA) at room temperature for 2 h. Subsequently, cells were incubated with mouse anti-sarcomeric alpha actinin (1:200) and rabbit anti-CX43 (1:500) at 4 °C overnight. After being washed with PBS 3 times, cells were incubated with Alexa Fluor 488 donkey anti-mouse IgG (H&L, 1:500) and Alexa Fluor 568 donkey anti-rabbit IgG (H&L, 1:500) for 2 h at room temperature. Cells were then washed with PBS and stained with 4′, 6-diamidino-2-phenylindole (DAPI) for 1 h and then imaged with confocal microscopy (LSM 880 with Airyscan). The area fraction of α-actinin-positive cells was quantified using ImageJ software. Each sample was performed in triplicate, and at least four fields per sample were used for quantification. For the F-actin staining, cells were rinsed with PBS and fixed with 4% paraformaldehyde for 20 min. Next, the cells were stained with 500 nM fluorescein isothiocyanate phalloidin (AAT Bioquest) for 20 min and stained with DAPI followed by rinsing with PBS. Fluorescence images were captured by confocal microscopy.

Western blot analysis

After culturing for 7 days, CMs on scaffolds were washed three times with PBS. Cells were ground in liquid nitrogen, and the total proteins were extracted using RIPA protein extraction solution. Total protein concentrations were measured by BCA Protein Assay (KeyGEN, China). The proteins (20 µg per lane) were separated on 10% SDS-PAGE and electrophoretically transferred onto PVDF membranes, which were blocked with 5% skim milk (w/v) in TBS-T buffer (10 mM Tris HCl, pH 7.5, 500 mM NaCl, 0.05% Tween 20) for 2 h at room temperature and then incubated with primary antibody against α-actinin or CX-43 at 4 °C overnight. Membranes were then washed 3 times with TBS-T (10 min each time) and incubated with the corresponding HRP-linked secondary antibody for 2 h at room temperature. The signals were detected by Super ECL Detection Reagent (Shang Hai Yeasen Biological Technology, China) according to the manufacturer's instructions. GAPDH was used as an internal control. The experiments were performed for three independent biological replicates and the data were analyzed with ImageJ software.

Morphological observation

Morphological observation of CMs on the scaffolds was performed with SEM. After culturing for 7 days, CMs on scaffolds were washed 3 times with PBS and fixed with 0.1% formaldehyde overnight. The fixed cells were rinsed with PBS, dehydrated with an ethanol series (50%, 60%, 70%, 80%, and 90%, and 95% once each for 5 min and finally twice with 100% for 5 min) and air-dried. Cells were stained with dioxin and lead citrate. Images were captured with SEM.

Calcium transient imaging and contraction activity of dopa-based ES-P50 ECP

After co-culturing for 3 or 7 days, CMs on membranes were stained with Fluo-4 AM reagent (Molecular Probes) to visualize the calcium current's traverse at 37 °C for 45 min according to the manufacturer's instructions. After staining, cells were washed with PBS, and then calcium current fluorescence was measured with a fluorescence microscope. Fluorescence (F) was normalized to

background intensity (F_0) during cell contraction and was plotted over the time course with ImageJ software. Calcium transients were calculated according to a reported method [49]. Ten successive F/F0 peaks in four selected zones per sample were used for calculating the parameter of time to peak, and the peaks in three time periods (5 s per time period) in four selected zones per sample were used to quantify the peak number within 5 s. Three independent samples per group were quantified. The contraction activity and the moving activity of the dopa-based ES-P50 ECP were recorded with a video capture program (Panasonic, HC-X900M, Japan). The video sequences were digitized at a rate of 25 frames per second, and the beating signals and moving signals were analyzed and recorded by MATLAB [50]. The trajectories of beating and displacement were graphed using OriginPro 8.0 software, based on the signal data derived from MATLAB. At day 7, the mean beating frequency of dopa-based ES-P50 ECP, which was obtained from 5 different time periods (2 min per time period), was quantified by ImageJ software.

Cell proliferation and vascularization on ES membranes

The cell proliferation of HUVECs cultured on membranes was assessed through Ki67 immunostaining. The vascularization of HUVECs on membranes was analyzed through vWF immunostaining and quantitative real-time reverse-transcription polymerase chain reaction (qRT-PCR) for the expression of related genes. After culturing for 1 day, the immunostaining of Ki67 or vWF of HUVECs on membranes was performed using mouse anti-Ki67 antibody (1:200) or rabbit anti-vWF antibody (1:200). Each experiment was performed in triplicate and at least four fields per sample were chosen. The proportion of Ki67+ cells and tube formation on membranes were counted using ImageJ software. After culturing for 3 days, total RNA of HUVECs on membranes was extracted for qRT-PCR assay with TRIzol Reagent (Ambion, Carlsbad CA, USA) according to the manufacturer's instructions. The cDNA was synthesized using Thermo First cDNA Synthesis Kit (Toyobo Co. Ltd., Japan) using standard procedures. qPCR was performed in triplicate with SYBR Green Master Mix kit (TaKaRa, Japan) and run on a StepOne PLUS system (Applied Biosystems, USA). Amplification conditions were as follows: hold at 95 °C for 10 min followed by 40 cycles for 15 s at 95 °C and 1 min at 60 °C. The output data were analyzed using the comparative ΔΔCt method. The results were normalized based on GAPDH mRNA expression, and then expressed as fold change compared with the control group (ES membrane). The sequences of PCR primers (forward and backward, 5' to 3') were as follows: VEGF, 5'-TGCGGATCAAACCTCACCA-3' and 5'-CAGGGATTTTTCTTGTCTTGCT-3'; KDR, 5'-GTGATCGGAAATGACACTGGAG-3' and 5'-CATGTTGGTCACTAACA GAAGCA-3'; eNOS, 5'-TGTCCAACATGCTGCTGGAAATTG-3' and 5'-AGGAGGTCTTCTTCCTGGTGATGCC-3'.

Animal experiments

Male SD rats (7-8 weeks, weight 250 ± 20 g) were divided into sham group (n=3) and MI group. The rats in the MI group were anesthetized with isoflurane. Ligation of the left anterior descending (LAD) artery was performed surgically as described in previous reports [31]. The rats in the sham group were subjected to a similar treatment except for the LAD ligation. After 14 days of LAD ligation, the rats whose fractional short-ending (FS) values were less than 30%, as evaluated by echocardiography, were divided into 5 subgroups (5 rats in each group). About 1.5 cm × 1.5 cm cardiac patches with or without CMs were then implanted onto the infarction area of the MI rats in 4 different transplantation groups. The edges of patches and the border of the epicardium of the infarct heart were sutured with 6-0 polypropylene sutures. For the sham and MI groups, the second thoracotomy was performed without ECPs transplantation. For immunosuppression, the rats received a daily subcutaneous injection of methylprednisolone (2 mg/kg), azathioprine (2 mg/kg), and methylprednisoline (2 mg/kg).

Echocardiography test

The left heart function of all animal groups was evaluated by IE33 echocardiography (Vevo2100, Visual Sonics). Two weeks after myocardial infarction and 4 weeks after patch transplantation, the rats were anesthetized, and transthoracic echocardiography was performed. M-mode echocardiography was recorded with a 40-MHz transducer, and short-axis views were obtained to measure the cardiac parameters. The cardiac functional parameters, including length of left ventricular internal diameter at end-diastole (LVIDd), length of left ventricular internal diameter at end-systole (LVIDs), left ventricular end-systolic volume (ESV) and left ventricular end-diastolic volume (EDV), ratio of stroke volume at left ventricular end diastolic volume (ejection fraction, EF), and (LVIDd-LVIDs)/LVIDs (fractional short-ending, FS) were measured.

Histological assay

Four weeks after transplantation, the rats were euthanized and their hearts were collected. The heart tissue was cut into 0.5 cm slices and fixed in 4%

paraformaldehyde for 4 h at room temperature. The slices were saturated with 30% sucrose for 2-3 days at 4 °C and embedded in O.C.T. for frozen sectioning. Subsequently, 5 µm sections were cut on a Leica CM1950 cryostat for Masson trichrome staining and immunostaining. The infarct areas were calculated using ImageJ software according to the ratio of the inner circumference length of the blue area to the entire inner circumference length in the LV by Masson trichrome staining. The wall thickness of the infarct area was measured with ImageJ software. The immunostaining for cardiac sections was performed according to the method used *in vitro*. The antibodies of mouse anti-α smooth muscle actin (α-SMA) (1:200), rabbit anti-CX-43 (1:200), and rabbit anti-F4/80 (diluted concentration: 1:200) were used.

Fluorescence detection of organs *ex vivo*

First, fluorescein isothiocyanate (FITC, BIOSHARP) was conjugated to GelMA polymer according to a reported method [51]. Briefly, 0.22 g gelatin was dissolved in 220 mL pH 9 Na_2CO_3-$NaHCO_3$ buffer solution, which was at 50 °C. Then, 22 mg fluorescein isothiocyanate was added to the gelatin solution and stirred at room temperature in the dark for 18 h. Finally, GelMA-FITC was obtained through dialysis and lyophilization. The procedure to synthesize FITC-conjugated GelMA-Ppy nanoparticles was similar to that of GelMA-Ppy nanoparticles. To minimize fluorescein photobleaching, the reaction and purification were performed in the dark. To examine the location of the transplanted patch in vivo, DiI-labeled CMs were co-cultured with the FITC-conjugated ES-P50 patch and then transplanted onto the infarcted area in MI rats for 4 weeks. Subsequently, the rats were sacrificed and their organs (heart, kidney, liver, lungs, spleen, etc.) were collected. The fluorescence signals in *ex vivo* organs were visualized by the IVIS Imaging system (Bruker FX Pro, USA).

Statistical analysis

All results were analyzed with SPSS22.0 and Origin 8.0 software. The data are expressed as mean ± standard deviation (SD). Statistical analyses were performed using one-way analysis of variance (ANOVA) with Tukey's post-hoc test. Differences were considered significant at $p < 0.05$.

Results

Characterization and biocompatibility of GelMA-Ppy nanoparticles

The morphology and size of GelMA-Ppy nanoparticles were assessed using TEM and DLS. The nanoparticles exhibited uniformly spherical structures (**Figure 1A**). DLS analysis revealed the narrow size distribution of GelMA-Ppy nanoparticles with an average size of 91.12 nm (**Figure S1A**). XRD results showed that the diffraction peaks were increased at $2\theta = 10°$ and $2\theta = 25°$, while the diffraction peak was decreased at $2\theta = 21°$ in GelMA-Ppy particles compared to pure Ppy and pure GelMA (**Figure 1B**), indicating the formation of the GelMA-Ppy polymer. The biocompatibility of GelMA-Ppy nanoparticles was assessed by live/dead staining of CMs. The cell viabilities of CMs (**Figure 1C**) and myocardial fibroblasts (**Figure S1C**) treated with 50 mg/mL GelMA-Ppy nanoparticles remained unchanged from day 1 to day 7. In contrast, many dead cells were detected on day 3 and day 7 in the control group treated with pristine Ppy. Quantitative analysis showed that more than 80% cells survived in CMs treated with GelMA-Ppy nanoparticles for 7 days, which was similar to the CMs cultured on glass slides, while only 60% CMs survived when treated with pristine Ppy (**Figure S1B**). Therefore, our prepared GelMA-Ppy nanoparticles had excellent biocompatibility and did not affect cell growth.

Characterization of mussel-inspired conductive membranes

To examine the ultrastructure of ES membranes, the surface was scanned by SEM. GelMA-Ppy nanoparticles were uniformly distributed, and the single fiber diameters were increased on the conductive layer of the mussel-inspired conductive membranes, including dopa-based ES-P10, ES-P20 and ES-P50 membranes (**Figure 2A2-4**). In the directly blending-spun ES-Ppy membrane, many aggregated Ppy particles were detected on the fibers (**Figure 2A5**). There was a color difference between ES-GelMA/PCL membrane (left side in **Figure 2B**) and dopa-based ES-P50 membrane (right side in **Figure 2B**). ES-GelMA/PCL membrane was white while dopa-based ES-P50 membrane was dark, indicating that GelMA-Ppy nanoparticles were uniformly distributed on the fibers of dopa-based ES-P50 membrane. The diameters of the conductive fibers were positively correlated with the quantity of GelMA-Ppy nanoparticles in the crosslinking solution, and the average fiber diameter of dopa-based ES-P50 membranes was 948 ± 153 nm (**Figure 2C**). The energy spectra of the membranes were also traced during the SEM observation. After the pristine ES-GelMA/PCL membrane was crosslinked with 50 mg/mL GelMA-Ppy nanoparticles through dopamine-MBA, the atomic ratio of the nitrogen element in the pristine ES-GelMA/PCL membrane was increased from 6.3% to 18.6% (**Figure S2A**). The higher concentration of
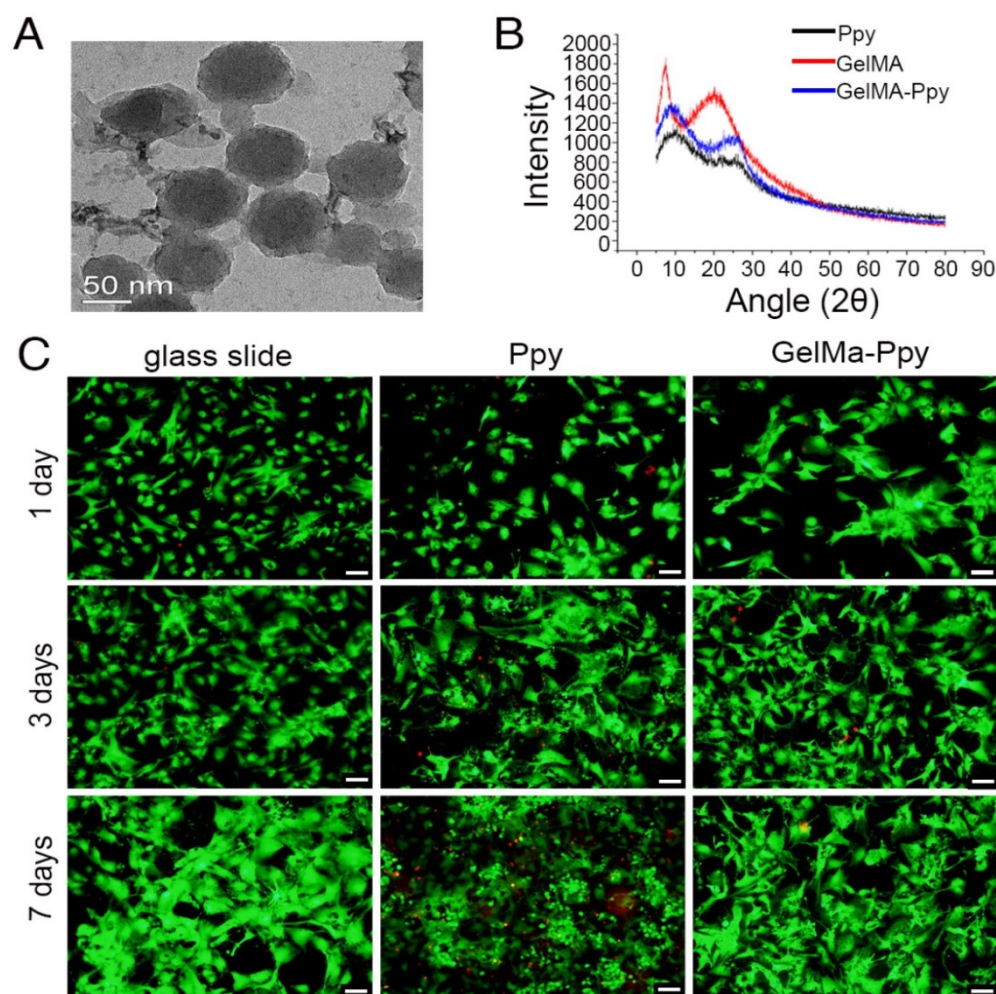
Figure 1. Characterization and biocompatibility of the GelMA-Ppy nanoparticles. (A) TEM image of GelMA-Ppy nanoparticles. (B) XRD analysis of GelMA-Ppy nanoparticles. (C) Live/dead staining of untreated CMs, 25 mg/mL Ppy-treated CMs, and 50 mg/mL GelMA-Ppy nanoparticles-treated CMs for 1, 3 and 7 days. The live cells are green and the dead cells are red. Scale bar, 50 μm.

GelMA-Ppy nanoparticles in mussel-inspired conductive membranes resulted in higher conductivity, reaching 0.3 S/m in the ES-P50 membrane (**Figure 2D**). The conductive layer produced a rough surface of ES fibers leading to contact angle changes. The contact angle of the dopa-based ES-P50 membrane was smaller than that of the pristine ES-GelMA/PCL membrane (**Figure 2E-F**). The rough surface of biomaterials was beneficial to cells spreading and growth (**Figure 2E-F**). There was more spreading of CMs on the dopa-based ES-P50 membranes than on the pristine ES-GelMA/PCL membranes on day 7 of culture.

Mussel-inspired conductive membranes promote CMs function *in vitro*

The viability of CMs cultured on ES membranes was investigated on days 1, 3, and 7 by the CCK-8 assay. The viability of CMs on pristine ES-GelMA/PCL membrane and conductive membranes was increased gradually over time (**Figure S2C**), indicating their excellent biocompatibility. CMs exhibited the highest cell viability when cultured for 3 and 7 days on the dopa-based ES-P50 membrane compared to those cultured on other membranes. The cell viability of CMs on the conductive membrane was higher than that on the pristine ES-GelMA/PCL membrane on day 7, while there was no significant difference in cell viability between CMs on dopa-based ES-P10 and ES-20 membranes. To investigate the influence of mussel-inspired conductive membranes on CMs function, cardiac-specific protein expression, calcium current traverse and synchronous contraction of CMs on different membranes were assessed. α-sarcomeric actinin is an important molecular marker for myocardial maturation and is closely related to the systolic function of CMs [52]. Connexin-43 (CX-43) protein is mainly responsible for the electric-contraction coupling of the myocardium [53, 54]. After 3 days of culture, the majority of CMs showed a round morphology without intact sarcomere formation on the pristine ES-GelMA/PCL

membrane (**Figure 3A1, C1**). However, typical sarcomeres formed in some CMs on mussel-inspired conductive membranes on day 3 (**Figure 3A2-5, C2-5**). After culturing for 7 days, a few mature CMs were observed on the pristine ES-GelMA/PCL membrane, while more elongated and highly packed sarcomeres formed on the conductive membranes (**Figure 3B, D**). Higher concentration of the crosslinked GelMA-Ppy nanoparticles induced a larger number of sarcomere structures and higher expression of α-sarcomeric

protein (**Figure 3B, D-F**) in CMs on ES membranes on day 7. Also, CX-43 protein was observed in inter-sarcomere and inter-cellular membranes (**Figure 3C-D**). The higher concentration of conductive nanoparticles in the conductive membrane yielded a higher expression of CX-43 protein in CMs on day 7 (**Figure 3G**). The sarcomeric α-actinin-positive area coverage on the dopa-based ES-P50 membrane reached about 30% and 55% on days 3 and 7, respectively (**Figure 3H**).
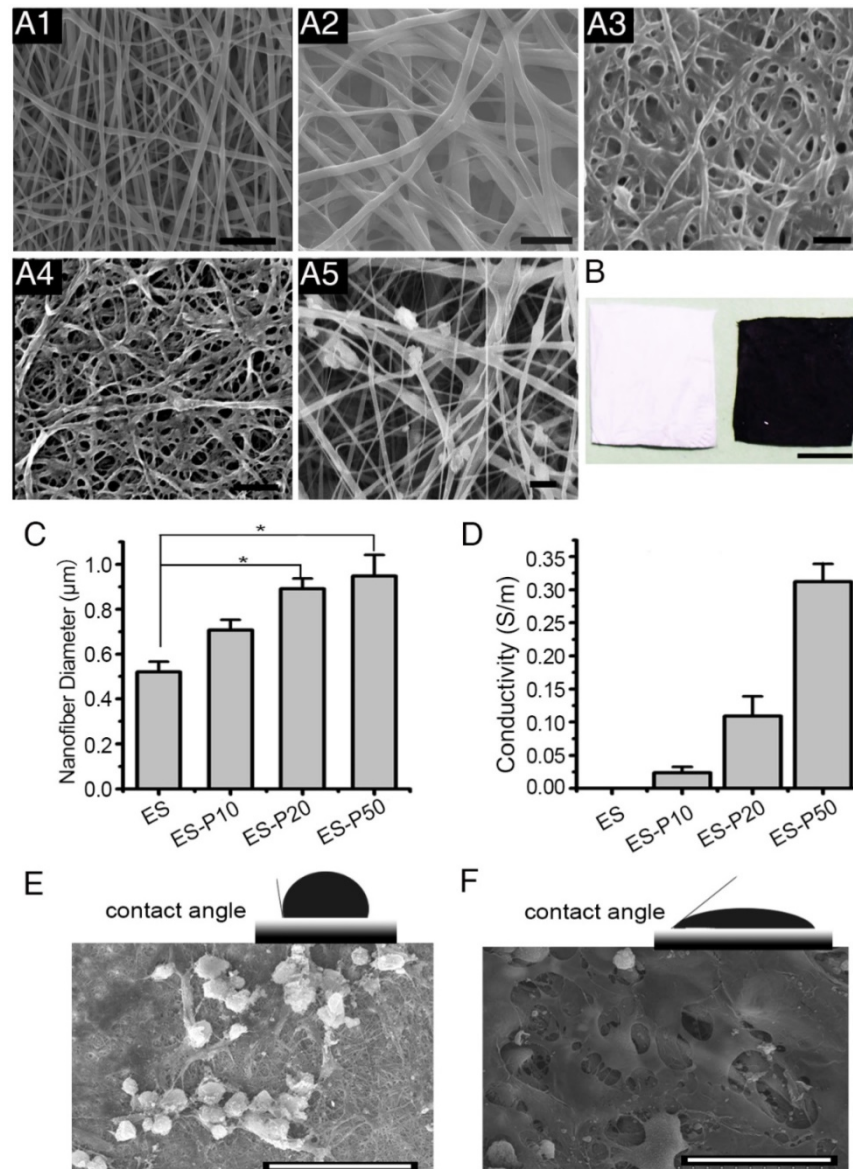

Figure 2. Characterization of the mussel-inspired conductive membranes. (A) SEM images of ES (A1), ES-P10 (A2), ES-P20 (A3), ES-P50 (A4), and ES-Ppy (A5). Scale bars, 5 μm. **(B)** Gross photographs of ES (white, left), and ES-P50 (dark, right). Scale bar, 5 mm. **(C)** Average fiber diameters of different membranes. All data are presented as mean ± SD. *p<0.05, n=3. **(D)** Conductivities of membranes. **(E-F)** The contact angles and outspread structure of CMs on ES (E), and on ES-P50 (F). ES: pristine ES-GelMA/PCL membrane; ES-P10: dopa-based ES-P10 membrane; ES-P20: dopa-based ES-P20 membrane; ES-P50: dopa-based ES-P50 membrane. ES-Ppy: directly blending-spun ES-Ppy membrane. Scale bars in (E-F), 50 μm.
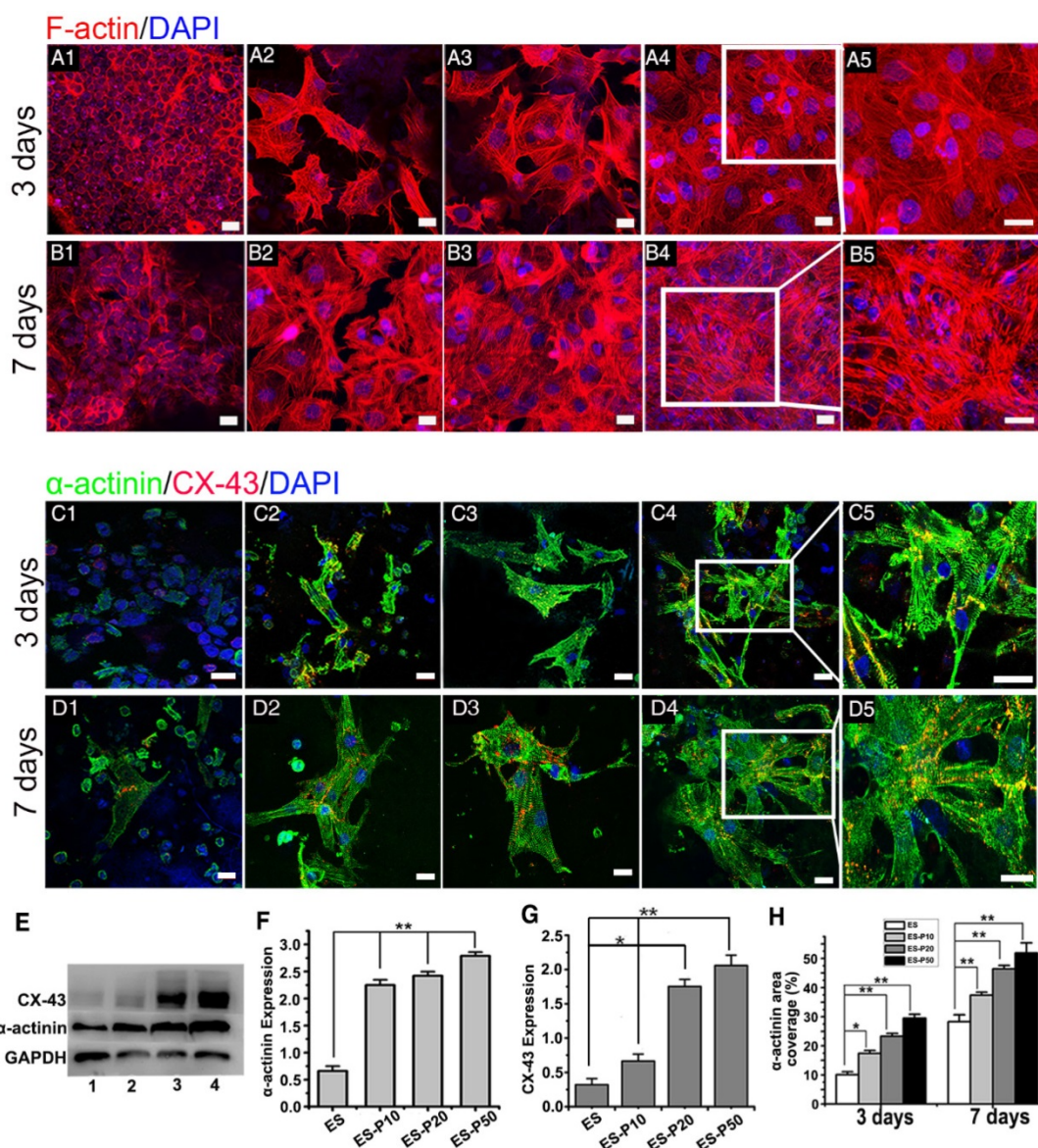
Figure 3. Mussel-inspired conductive membranes enhanced the function of CMs. (A-B) Filamentous actin (F-actin) staining for CMs on membranes on day 3 (A) and day 7 (B). (A1, B1) ES. (A2, B2) ES-P10. (A3, B3) ES-P20. (A4, B4) ES-P50. Scale bars, 20 μm. **(C-D)** α-actinin staining for sarcomere (green) and CX-43 proteins expression (red) of CMs on membranes on day 3 (C) and day 7 (D). (C1, D1) ES. (C2, D2) ES-P10. (C3, D3) ES-P20. (C4, D4) ES-P50. Scale bars, 20 μm. **(E)** Western blotting for the expressions of α-actinin protein and CX-43 protein in CMs on membranes on day 7 of culture. Line 1: ES. Line 2: ES-P10. Line 3: ES-P20. Line 4: ES-P50. **(F-G)** Quantitative analysis of α-actinin (F) and CX-43 (G) of CMs on membranes based on Western blotting. **(H)** α-actinin area coverage of CMs on membranes on day 3 and day 7 based on immunofluorescence. ES: pristine ES-GelMA/PCL membrane; ES-P10: dopa-based ES-P10 membrane; ES-P20: dopa-based ES-P20 membrane; ES-P50: dopa-based ES-P50 membrane. All data are presented as mean ± SD. *$p<0.05$, **$p<0.01$.

Intracellular Ca^{2+} mobilization is a key regulator of the physiological activity of CMs [52, 55]. The fluorescent Ca^{2+} indicator, Fluo-4 AM, was employed to track the calcium current traverse in CMs on different membranes through fluorescence signal detection. As presented in **Figure 4A-B** and **Movie S1**, intracellular Ca^{2+} spikes appeared synchronously, and parallel and rhythmic flows of calcium ions formed at different spots in the ECPs on day 7 with dopa-based ES-P20 and ES-P50. However, Ca^{2+} puffs in CMs at different places exhibited different frequencies in the ECP with pristine ES-GelMA/PCL, which had neither linear nor rhythmic patterns. A linear antegrade pattern of calcium flow also appeared in the ECP on

day 7 with dopa-based ES-P50. Quantitative parameters of calcium transient were calculated according to the results in **Figure 4A-B**. Shorter time to calcium peak and more peak numbers within 5 s of calcium transient in CMs appeared in the conductive ECPs compared to those in the ECP with pristine ES-GelMA/PCL (**Figure S3A-B**). The quantitative parameters of time to peak and peak numbers within 5 s represent the frequency of calcium transient. The ECP with dopa-based ES-P20 had a higher frequency of calcium transient in CMs than that with dopa-based ES-P10. Furthermore, among the conductive ECPs, the one with dopa-based ES-P50 exhibited the highest frequency of calcium transient in

CMs. There was no significant difference in the frequency of calcium transient in CMs seeded either on dopa-based ES-P20 or ES-P50. These results indicated that dopa-based conductive membranes, especially ES-P20 and ES-P50, could enhance inter-cellular communication among CMs.

High expression of cardiac-specific protein and rhythmic Ca^{2+} flow in CMs produce synchronous contraction of CMs. Throughout the whole ES-P50 ECP, the beating activity of CMs occurred at the same pace on day 7. Synchronous contraction, even spontaneous movement toward one direction of ES-P50 ECP, could be visualized by the naked eye

(**Figure 4C** and **Movie S2**). The movement displacement and beating signals of ES-P50 ECP displayed in **Figure 4C** were recorded and analyzed with MATLAB and ImageJ software. The moving trajectory of the rectangle swimmer (ES-P50 ECP) and its travel velocity was about 24 mm/min (**Figure S3C**). The results suggested that this ES-P50 ECP could have potential as a biohybrid actuator. The spontaneous cyclic extension/contraction was observed in ES-P50 ECP, and the mean beating frequency of ES-P50 ECP was 150 ± 7.071 beats/min on day 7 (**Figure S3D**).
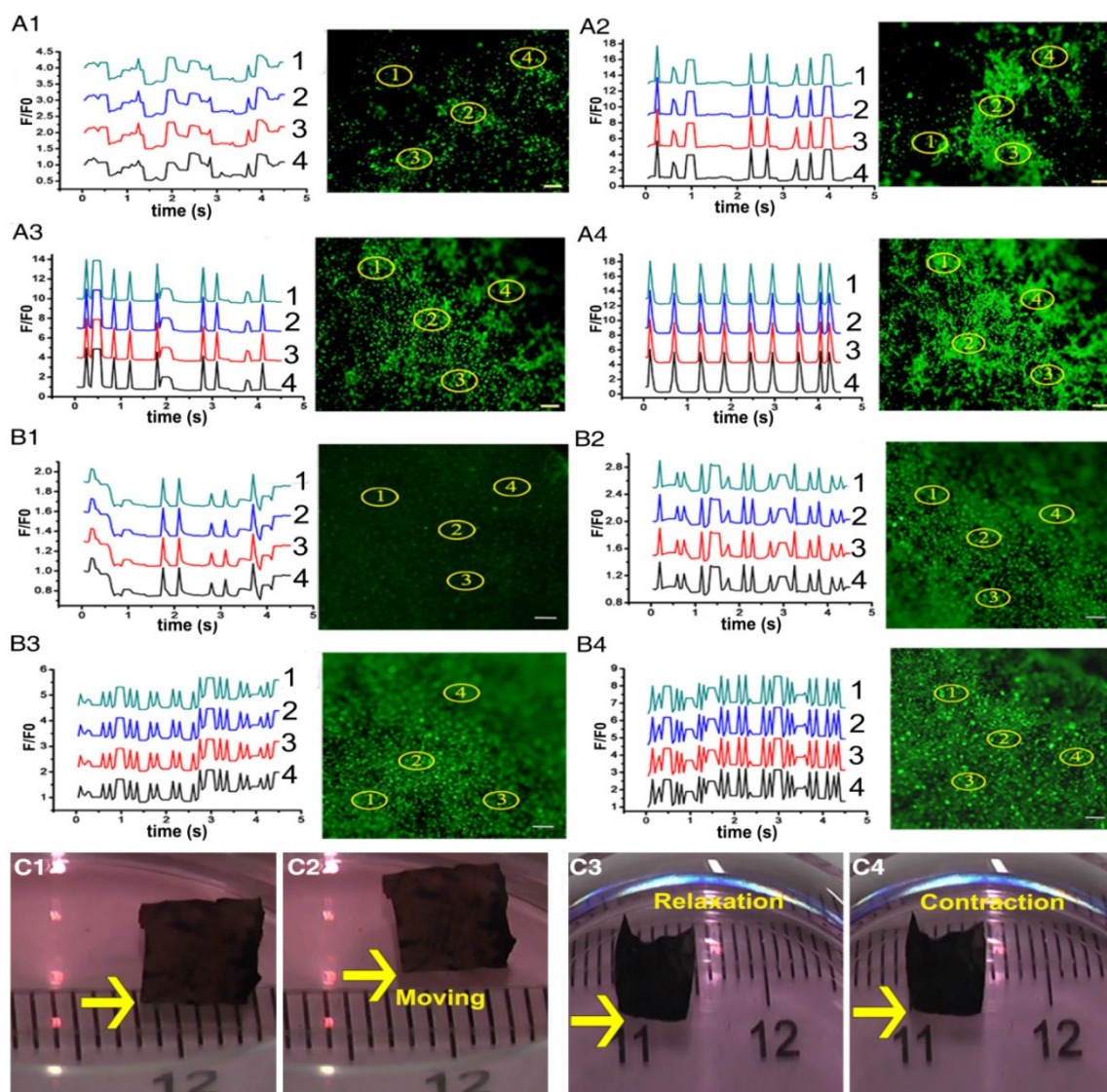

Figure 4. Dopa-based conductive membranes increase calcium transient's frequency within CMs and spontaneous movement of ECPs. (A-B) Transient and extracted frequency signals of Ca^{2+} within CMs on membranes on day 3 (A) and day 7 (B). (A1, B1) Pristine ES-GelMA/PCL membranes. (A2, B2) Dopa-based ES-P10 membranes. (A3, B3) Dopa-based ES-P20 membranes. (A4, B4) Dopa-based ES-P50 membranes. Scale bars, 100 μm. (C) Spontaneous movement (C1-C2) and contraction activity (C3-C4) of dopa-based ES-P50 ECPs on day 7.
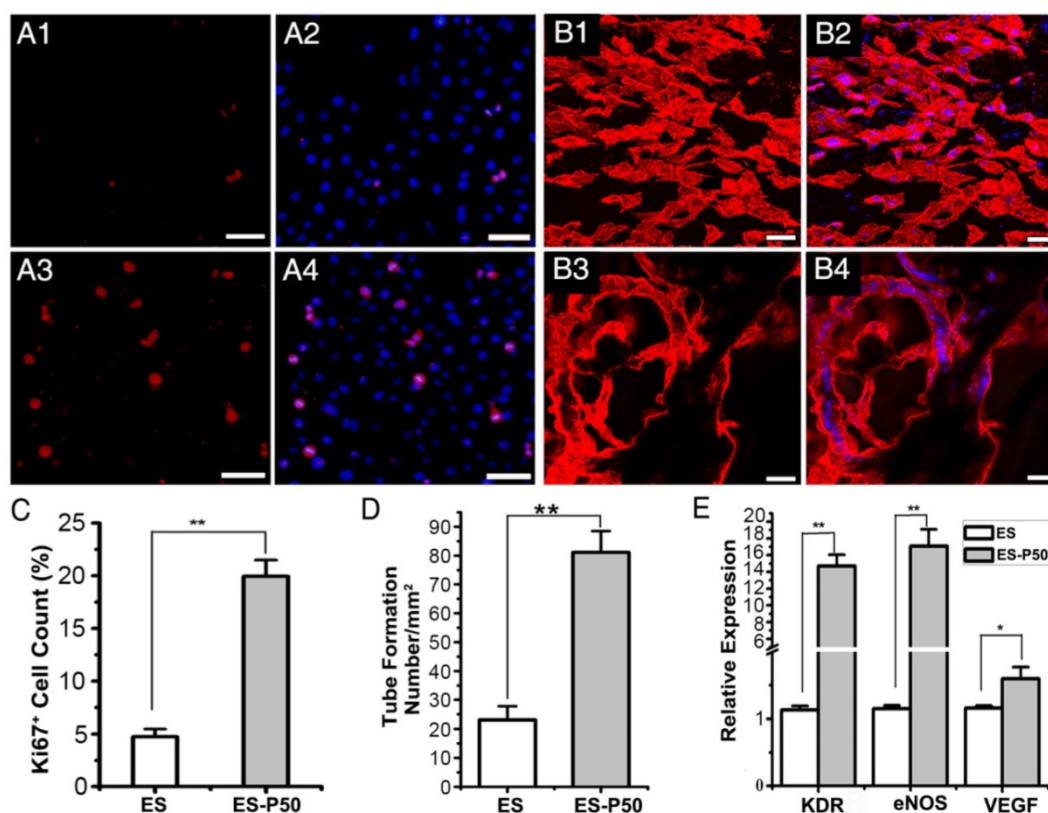
Figure 5. ES-P50 membrane was beneficial for the proliferation and vascularization of HUVECs *in vitro*. (A) Ki67-positive cells (red) on ES (A1-A2) and ES-P50 (A3-A4). Scale bars, 50 µm. **(B)** vWF-positive HUVECs (red) on ES (B1-B2) and ES-P50 (B3-B4). Scale bars, 20 µm. **(C)** Percentage of Ki67-positive cells on ES and ES-P50. **(D)** Tube number per mm^2 formed by HUVECs on ES and ES-P50. **(E)** Expression of KDR, eNOS and VEGF genes in HUVECs on ES and ES-P50. ES: pristine ES-GelMA/PCL membrane; ES-P50: dopa-based ES-P50 membrane. All data are presented as mean ± SD. *p<0.05, **p<0.01. n=3. Cell nuclei were stained with DAPI.

Mussel-inspired conductive nanofibrous membranes enhance cell proliferation and vascularization in ECP *in vitro*

To examine the effects of ES-P50 membrane on cell proliferation, Ki67 immunostaining of HUVEC cells was performed. The results revealed that the number of Ki67-positive HUVEC cells on ES-P50 membrane was about 4 times higher than that on the pristine ES-GelMA/PCL membrane after co-culturing for 6 h (**Figure 5A, C**). Co-culturing for 12 h followed by vWF immunostaining showed the formation of vascular-like organization on the dopa-based ES-P50 membrane but not on the pristine ES-GelMA/PCL membrane (**Figure 5B**). There was almost 3 times more tube formation/mm^2 on the dopa-based ES-P50 membrane than on the pristine ES-GelMA/PCL membrane (**Figure 5D**). Also, qRT-PCR analysis was performed to determine the effect of the membrane on the expression of angiogenic genes. There was a significant increase in the expression of angiogenic genes such as eNOS, VEGF, and its receptor KDR, in HUVECs cultured on the ES-P50 membrane compared to those on the pristine ES-GelMA/PCL membrane (**Figure 5E**). These results indicated that mussel-inspired conductive nanofibrous membranes

enhanced cell proliferation and vascularization in ECP.

Mussel-inspired conductive ECP repairs infarct myocardium by enhancing cardiac function and revascularization

To determine if the mussel-inspired conductive ECP with or without CMs could repair infracted myocardium, the effects of ECP were systematically investigated following transplantation for 4 weeks. Cardiac sections were stained with Masson's trichrome and immunostained with antibodies against α-actinin and CX-43. The patch-implanted groups possessed more myocardial tissues in infracted areas while fibrous tissues were observed in the MI group (**Figure 6A-G**). Higher expressions of α-actinin and CX-43 were observed in the patch-implanted heart compared to those in the MI heart (**Figure 6B-G**). The infarct size was significantly different among the groups: 30.04% ± 0.11% in the MI group, 27% ± 1.24% in the pristine ES-GelMA/PCL membrane group, 24.32% ± 0.48% in the pristine ES-GelMA/PCL ECP group, 20.65% ± 0.83% in the dopa-based ES-P50 membrane group, and 13.41% ± 0.78% in the dopa-based ES-P50 ECP group (**Figure 6H**). The dopa-based ES-P50 ECP group had the smallest infarct size and the thickest ventricle wall

among the 4 patch-implanted groups (**Figure 6H-I**). Cardiac functions among various groups were evaluated by echocardiography on day 28 after transplantation. The echocardiographic images showed that obvious contraction waves of LV appeared in the dopa-based ES-P50 ECP group (**Figure 7A**). The parameters in various groups calculated by echocardiography are shown in **Figure 7B-G**. The parameters EF% (**Figure 7B**) and fraction shorting (FS%) (**Figure 7C**) represent the LV's capability for pumping blood. The parameters LVIDd (**Figure 7E**), LVIDs (**Figure 7D**), ESV (**Figure 7F**), and EDV (**Figure 7G**) express the LV's contraction function. All patch transplantations increased the cardiac function of the infarcted heart. The dopa-based ES-P50 membrane transplantation yielded higher EF%, lower LVIDs and lower ESV compared to the pristine ES-GelMA/PCL membrane transplantation. The dopa-based ES-P50 ECP transplantation significantly strengthened the LV's EF% by about 30% and LV's FS% by about 20% (**Figure 7B-C**). The dopa-based ES-P50 ECP transplantation induced the strongest contraction function of LV among the patch-transplantation groups (**Figure 7**).

To know the effects of different patches for revascularization in the infarct area, H&E staining and dual immunostaining for vWF and α-SMA were performed. Vascular structures, including vWF+ micro-vessel network and arterioles derived from the co-localization of vWF+ and α-SMA+ proteins, in all patch-implanted groups were denser than those in the MI group (**Figure 8**). The vessel density was assessed as the number of vWF+ vessels per mm². The density of vessels in the infarct area in the dopa-based ES-P50 membrane group was higher than that in the pristine ES-GelMA/PCL membrane and the pristine ES-GelMA/PCL ECP group. The ES-P50 ECP group had the highest vascularization. Our results indicate that the mussel-inspired conductive ECP repaired infarct myocardium by enhancing cardiac function and revascularization.
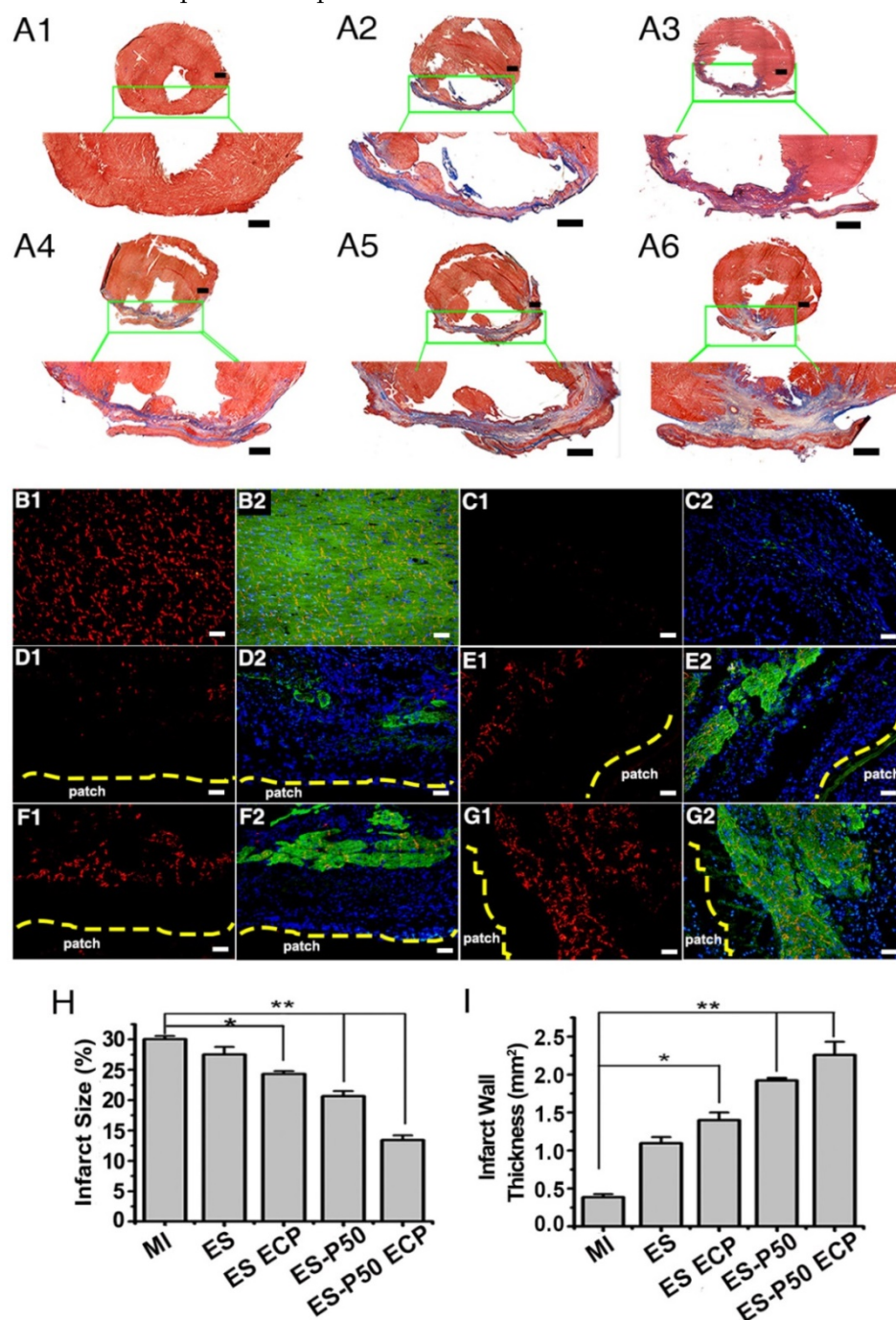

Figure 6. Mussel-inspired conductive membranes were effective for infarct myocardium repair. (A) Masson's staining for fibrous tissue (blue) and myocardium (red) of heart sections in rats. (A1) Sham group. (A2) MI group. (A3) ES group. (A4) ES ECP group. (A5) ES-P50 group. (A6) ES-P50 ECP group. Scale bars, 1 mm. **(B-G)** α-actinin-positive myocardial tissue (green) and CX-43 protein expression (red) in the infarcted area. (B1-B2) Sham group. (C1-C2) MI group. (D1-D2) ES group. (E1-E2) ES ECP group. (F1-F2) ES-P50 group. (G1-G2) ES-P50 ECP group. Cell nuclei were stained with DAPI. Scale bars, 50 μm. **(H-I)** Statistical analysis of infarct size (H) and infarct wall thickness (I). ES: pristine ES-GelMA/PCL membrane group; ES-ECP: pristine ES-GelMA/PCL ECP group; ES-P50: dopa-based ES-P50 membrane group; ES-P50 ECP: dopa-based ES-P50 ECP group. All data are presented as mean ± SD. *p<0.05, **p<0.01.

Inflammation responses and biocompatibility of ES-P50 ECP *in vivo*

After the patches were transplanted into the infarcted hearts for 28 days, the inflammation responses in various groups were investigated with F4/80 as a major macrophage marker. The number of F4/80-positive cells did not increase (**Figure 9A6**), suggesting that transplantation of the patches did not induce an excess of inflammation infiltration. However, pristine ES-GelMA/PCL ECP transplantation, dopa-based ES-P50 membrane transplantation, and dopa-based ES-P50 ECP transplantation significantly decreased the number of macrophagocytes in infarct areas. To locate the

transplanted patch *in vivo*, FITC-conjugated GelMA/PCL ES membrane and FITC-conjugated GelMA-Ppy nanoparticles were synthesized. On day 28 after transplantation, the heart and other vital organs (such as lungs, spleen, liver and kidneys) in dopa-based ES-P50 ECP-transplanted rats were collected, and the fluorescence signals derived from the FITC-conjugated GelMA in dopa-based ES-P50 membrane and the DiI-labeled transplanted CMs in ECP were assessed by the IVIS Imaging system (Bruker FX Pro, USA). As shown in **Figure 9B**, strong signals, including FITC-positive fluorescence and DiI-positive fluorescence, were observed in the patch-transplanted heart, but not in other organs.
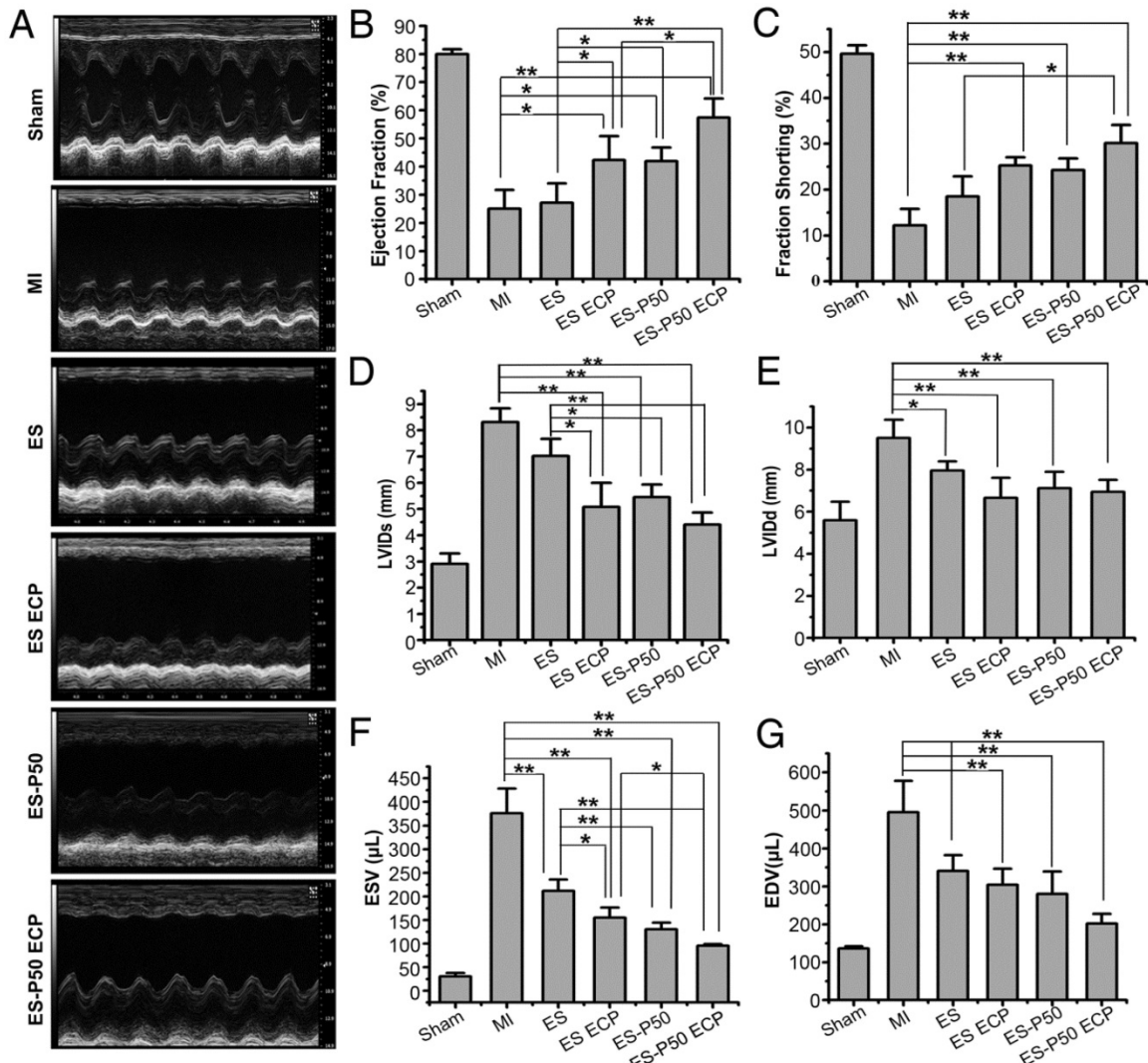

Figure 7. Left ventricular function determined by echocardiography 4 weeks after transplantation. (A) Representative echocardiographic images. **(B-G)** Representative parameters of left ventricular function based on echocardiography. ES: pristine ES-GelMA/PCL membrane group; ES ECP: pristine ES-GelMA/PCL ECP group; ES-P50: dopa-based ES-P50 membrane group; ES-P50 ECP: dopa-based ES-P50 ECP group. All data are presented as mean ± SD. *p<0.05, **p<0.01.
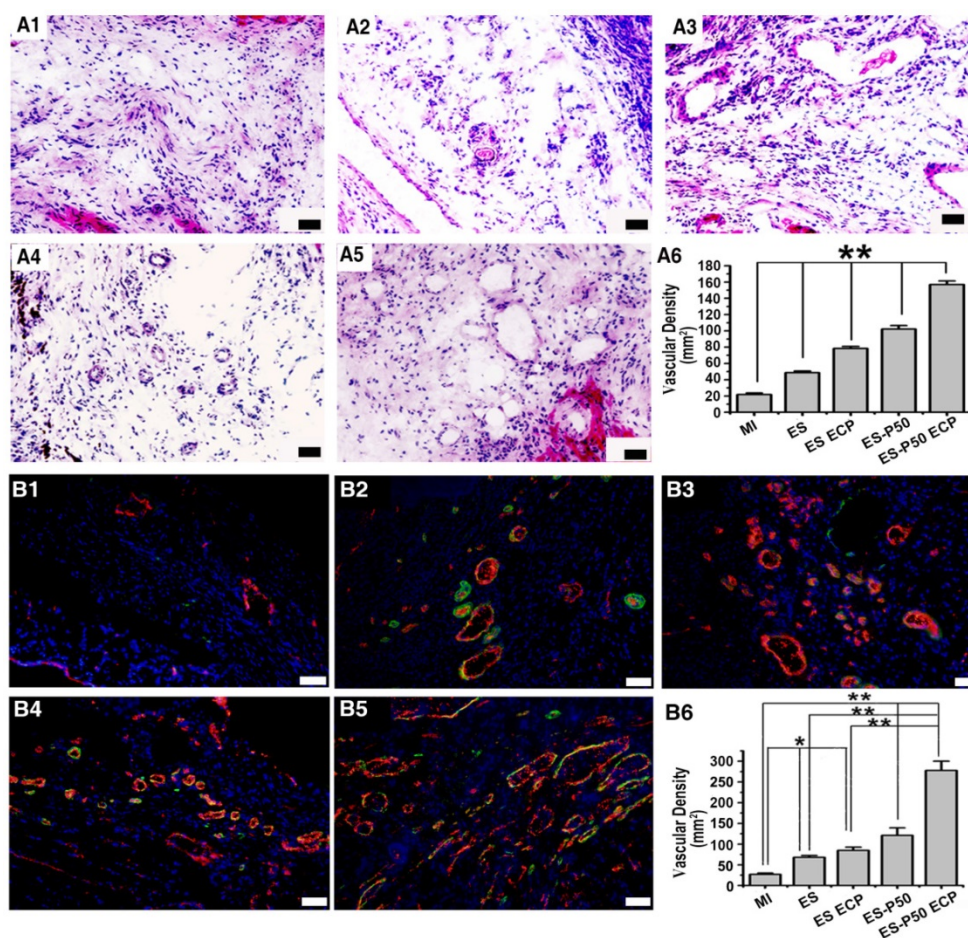
Figure 8. Mussel-inspired conductive ECP enhanced vascularization of infarct myocardium. (A) H&E staining of the infarct area in the MI group (A1), ES group (A2), ES ECP group (A3), ES-P50 group (A4), and ES-P50 ECP group (A5). Scale bars, 50 µm. (A6) Microvessel density within infarcted myocardium based on H&E staining. All data are presented as mean ± SD. **p<0.01. n=3. **(B)** vWF immunostaining (red) and α-SMA immunostaining (green) of the infarct area in the MI group (B1), ES group (B2), ES ECP group (B3), ES-P50 group (B4), and ES-P50 ECP group (B5). Scale bars, 50 µm. (B6): Microvessel density within infarcted myocardium based on vWF immunostaining. ES: pristine ES-GelMA/PCL membrane group; ES ECP: pristine ES-GelMA/PCL ECP group; ES-P50: dopa-based ES-P50 membrane group; ES-P50 ECP: dopa-based ES-P50 ECP group. All data are presented as mean ± SD. *p<0.05, **p<0.01.

Discussion

In this study, we sequentially synthesized GelMA-Ppy nanoparticles and dopa-grafted ES-GelMA/PCL membrane and then developed a dopa-based conductive membrane using simple ultrasonic concussion. The GelMA-Ppy nanoparticles and the dopa-based conductive membranes were biocompatible and highly conductive. This dopa-based conductive membrane was beneficial for CMs function and synchronous contraction *in vitro* as well as effective for repairing infarct myocardium *in vivo*.

Herein, we employed paratoluenesulfonic acid (pTS) and $FeCl_3$ as the dopant and the oxidizing agent, respectively, for the formation of Ppy. During the process of oxidative polymerization of Ppy, the pendant methacrylate groups of GelMA formed a self-crosslinked network [4, 56], helping the formation of spherical GelMA-Ppy nanoparticles. It seems that Ppy does not provide cell-interactive moieties, and the self-crosslinked network of GelMA-Ppy improves the cytocompatibility of Ppy [43, 57]. The

incorporation of GelMA in GelMA-Ppy nanoparticles was bifunctional, keeping the nanoparticles conductive and promoting cell survival. As shown in **Figure 1C** and **Figure S1B-C**, the cardiac cells maintained excellent cell viability after being challenged with GelMA-Ppy nanoparticles for 7 days even at the high concentration of 50 mg/mL.

It has been reported that ES-produced nanofibers structurally mimic the cardiac extracellular matrix (ECM) [58, 59], and nanofibers containing conductive polymer closely resemble the native myocardial microenvironment [28]. PCL provides the strong and ductile mechanical property of nanofibers [60]. GelMA incorporation can not only improve the biocompatibility of fibers but also offers pre-crosslinked groups with dopamine-MBA. In this study, a pristine ES-GelMA/PCL nanofibrous membrane was produced. GelMA-Ppy nanoparticles were then concussively crosslinked onto the pristine ES-GelMA/PCL nanofibers using the dopamine-MBA crosslinker to form dopa-based conductive nanofibers. During the mechanical concussion, the

GelMA-Ppy nanoparticles in the liquid were uniformly distributed on the surface of ES-GelMA/PCL nanofibers and then crosslinked through dopamine-MBA. After crosslinking with GelMA-Ppy nanoparticles, the mean diameter of the ES-GelMA/PCL nanofibers of the dopa-based ES-P50 membrane was increased from 520 ± 45.81 nm to 948 ± 153 nm. The dopa-based ES-P50 membrane yielded high conductivity (0.3 S/m), which was higher than that of direct blending of ES with pure Ppy and PCL [28] and is also higher than that of Ppy directly deposited onto PCL electrospun membrane [29]. The conductivity of this dopa-based ES-P50 membrane was closer to the natural ventricular myocardium (1.0-2.0 S/m) than other reported Ppy-incorporated ES membranes [61].

Besides its high conductivity, the dopa-based ES-P50 membrane also displayed good biocompatibility and was beneficial for the spreading, growth, and function of CMs. In a previous study, incorporation of pure Ppy increased the hydrophobicity of the scaffolds [28]. In this study, GelMA-doped Ppy nanoparticles exhibited hydrophilicity, leading to the smaller contact angle (36.8° ± 1.39°) of the dopa-based ES-P50 membrane compared to that of the pristine GelMA/PCL membrane. Contact angle reflects the hydrophilicity of scaffolds, which influences protein adsorption and cell attachment [62]. Furthermore, dopamine-MBA can preserve dopamine's adhesive capability besides its crosslinking function on the dopa-based ES-P50 membrane, improving cell attachment and cell spreading. Therefore, as shown in **Figure 2E-F** and **Figure S2C**, the hydrophilic and rough surface of the dopa-based ES-P50 membrane was better for cell attachment, cell spreading, and cell viability of CMs compared to the hydrophobic and smooth surface of the pristine ES-GelMA/PCL membrane.

Reinforced electrical conduction in scaffolds is beneficial to CM function and synchronous contraction [7, 63, 64]. Our results also suggest that the dopa-based conductive membranes are better for the formation of sarcomeres in CMs. Compared to the pristine ES-GelMA/PCL membrane, the concentration of crosslinked conductive nanoparticles in the dopa-based conductive membranes was positively correlated with the maturity of CMs. Furthermore, Ca^{2+} transient propagation served as an indicator of action potential propagation. Our results suggest that the dopa-based conductive membranes could promote Ca^{2+} transient propagation among CMs, and, compared to the other membranes, the dopa-based ES-P50 membrane induced faster electric diffusion between CMs. Thus, the dopa-based conductive membranes were effective conductive scaffolds for ECP construction.
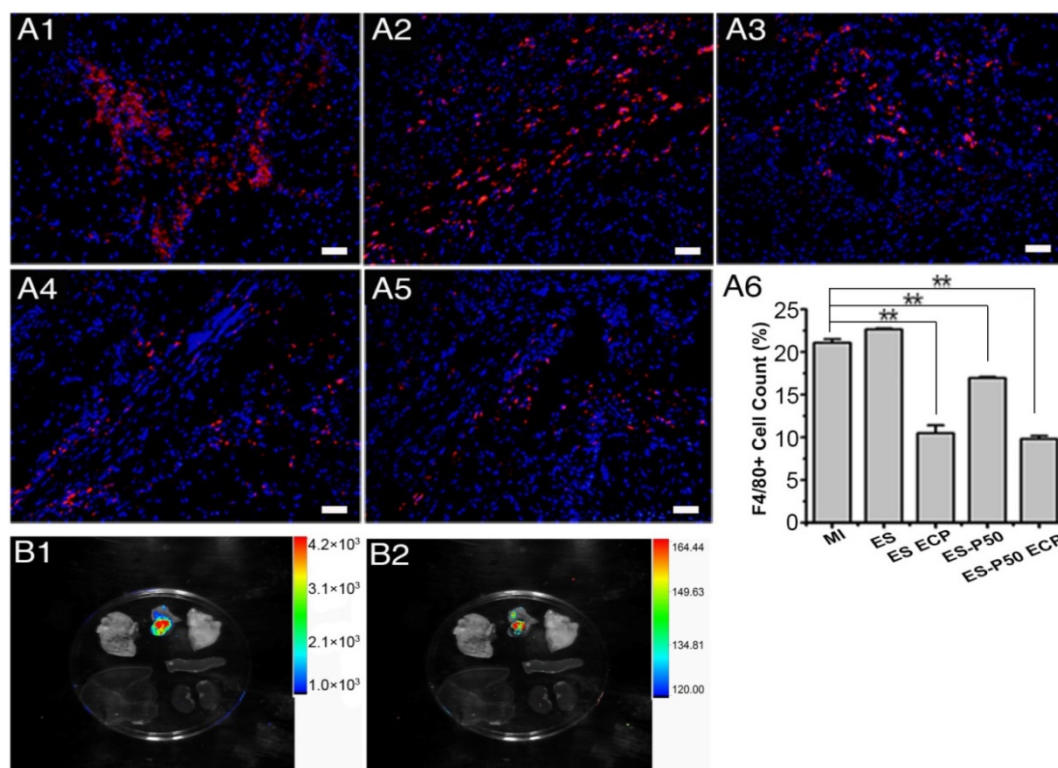

Figure 9. Inflammation in the infarcted area after patch transplantation, and the location of the dopa-based ES-P50 ECP *ex vivo* 4 weeks after transplantation. (A) F4/80 immunostaining in MI group (A1), ES group (A2), ES ECP group (A3), ES-P50 group (A4) and ES-P50 ECP group (A5). Scale bars, 50 μm. **(A6)** F4/80-positive cells in different groups. ES: pristine ES-GelMA/PCL membrane group; ES ECP: pristine ES-GelMA/PCL ECP group; ES-P50: dopa-based ES-P50 membrane group; ES-P50 ECP: dopa-based ES-P50 ECP group. All data are presented as mean ± SD. **p<0.01. **(B)** Fluorescence from FITC-marked scaffold signal (B1) and DiI-positive CMs signal (B2) in different organs.

We further investigated the repair effect of dopa-based ES-P50 membrane for infarct myocardium. Four weeks after transplantation of dopa-based ES-P50 ECP into the infarcted heart, the conductive nanoparticles in ECP did not transfer into other organs and the transplanted patch did not induce an excess of inflammation infiltration in the infarcted heart. Our results revealed that compared to the MI group, the dopa-based ES-P50 membrane transplantation reduced the infarct area by 31%. Furthermore, the dopa-based ES-P50 ECP transplantation significantly reduced the infarct area by about 50% compared to the MI group. The dopa-based ES-P50 ECP enhanced cardiac function and revascularization in the infarct area. After MI, the loss of electric unification between infarct tissue and normal myocardium results in ventricular dysfunction and heart failure. The conductive polymer-incorporated scaffold improved the cardiac function of the infarcted heart by accelerating conduction velocity and repolarization in the peri-infarct area [29], which restored the lost electrical conductivity and synchronous contraction of the scar tissue [52]. Our *in vitro* data showed that dopa-based ES-P50 membrane was a functional conductive scaffold for CMs. Hence, dopa-based ES-P50 membrane-derived ECP acted as a mediator to enhance electrical integration between the scar tissue and normal myocardium, inducing myocardium regeneration with similar myocardium structure and enhanced cardiac function of the infarcted heart. The regenerated myocardium in the infarct area induced by the dopa-based ES-P50 ECP transplantation had a structure similar to normal heart and the dense presentation of CX-43 in the regenerated myocardium is indicative of the normal electric-contraction function of the regenerated myocardium [53, 54]. Angiogenesis plays a critical role in infarcted myocardial repair. Neovascularization in the infarct tissue facilitates metabolic balance and the restoration of cardiac function [65]. It is important for the functional ECP to improve vascularization in the infarcted tissue. Compared to two-dimensional microenvironment, three-dimensional microenvironment confers more physiological cues for vascular endothelial cells to be aligned well and form vascular network-like structures [66]. The ES membrane has a two-dimensional analogous architecture and, therefore, is adverse for vascularization. In this study, after the GelMA-Ppy nanoparticles were crosslinked onto the pristine ES membrane, more vascular-like structures appeared on the dopa-based ES-P50 membrane compared to that on the pristine ES-GelMA/PCL membrane. The conductive scaffold enhanced vascularization in the infarct area during the process of infarcted myocardial repair [67]. Consistent with this observation, our data *in vivo* confirmed that dopa-based conductive membrane-derived ECP had angiogenesis function *in vivo*. These results suggest that dopa-based ES-P50 ECP could effectively repair infarct myocardium through enhancing cardiac function and revascularization.

Conclusion

Herein, conductive and spherical GelMA-Ppy nanoparticles were synthesized that displayed excellent biocompatibility. More than 80% of CMs survived treatment with GelMA-Ppy nanoparticles after 7 days of culture. GelMA-Ppy nanoparticles, even at the high concentration of 50 mg/mL, could be uniformly crosslinked onto the ES nanofibers by dopamine-MBA crosslinker and a simple ultrasonic concussion without obvious aggregation. However, either direct blending-ES of Ppy/PCL or direct deposition of Ppy on PCL electrospun membrane produced apparent aggregation of particles on ES nanofibers. The higher concentration of GelMA-Ppy nanoparticles yielded high membrane conductivity (0.3 S/m), which is much higher than that of other conductive Ppy-incorporated membranes produced by conventional methods. The dopa-based ES-P50 membrane had good biocompatibility after transplantation without obvious immune response and reduced inflammatory infiltration in the infarcted area. The dopa-based ES-P50 membrane also exhibited optimal performance for function and synchronous contraction of CMs as well as Ca^{2+} current propagation among CMs. The conductive GelMA-Ppy nanoparticles modified the surface topography of the pristine ES-GelMA/PCL membrane to promote vascularization of HUVECs *in vitro*. Interestingly, even the dopa-based ES-P50 conductive membrane without CMs reduced myocardial infarction via revascularization *in vivo*. Therefore, the dopa-based ES-P50 conductive membrane with CMs (ES-P50 ECP) was more effective in repairing the infarcted myocardium through exogenous CMs and revascularization in the infarct zone. In this study, we reported a facile, cost-economical, and effective approach to fabricate a conductive nanofibrous membrane, which can be a promising candidate scaffold for cardiac patch engineering for MI repair.

Abbreviations

DAPI: 4′, 6-diamidino-2-phenylindole; DiI: chlormethylbenzamido-1,1-dioctadecyl-3,3,3′3′-tetra methylin-docarbocyamine; DLS: dynamic light scattering; dopa-based ES-P10 membrane:

dopa-grafted ES-GelMA/PCL membrane crosslinked with 10 mg/mL GelMA-Ppy; dopa-based ES-P20 membrane: dopa-grafted ES-GelMA/PCL membrane crosslinked with 20 mg/mL GelMA-Ppy; dopa-based ES-P50 membrane: dopa-grafted ES-GelMA/PCL membrane crosslinked with 50 mg/mL GelMA-Ppy; ECM: extracellular matrix; ECP: engineered cardiac patch; EDV: end-diastolic volume; ESV: end-systolic volume; FITC: fluorescein isothiocyanate; GelMA: methylacrylic anhydride-gelatin; GelMA-Ppy: methylacrylic anhydride-gelatin-modified Ppy; HUVECs: human umbilical vein endothelial cells; LAD: left anterior descending; LVFS: left ventricular shortening fraction; LVIDd: left ventricular internal diameter at end-diastole; LVIDs: left ventricular internal diameter at end-systole; MA: methylacrylic anhydride; MBA: N'N'-methylene-bis-acrylamide; PCL: polycaprolactone; pTS: paratoluenesulfonic acid; PEGDA: poly (ethylene glycol) diacrylate; Ppy: polypyrrole; PVDF: polyvinylidene fluoride; qRT-PCR: quantitative real-time reverse-transcription polymerase chain reaction; SDS-PAGE: sodium dodecyl sulfate polyacrylamide gel electrophoresis; SEM: scanning electron microscopy; TEM: transmission electron microscopy; vWF: von Willebrand Factor; XRD: X-ray diffraction.

Supplementary Material

Figure S1 indicates the biocompatibility of GelMA-Ppy nanoparticles. **Figure S2** indicates the characterization of dopa-based conductive membranes. **Figure S3** indicates the calcium transient parameters of CMs cultured on different membranes.
http://www.thno.org/v08p5159s1.pdf
Movie S1 displays the Ca²⁺ traverse in CMs cultured on different membranes.
http://www.thno.org/v08p5159s2.mp4
Movie S2 displays the synchronous movement of the ES-P50 ECP.
http://www.thno.org/v08p5159s3.mp4

Acknowledgments

Competing Interests

The authors have declared that no competing interest exists.

References

1. Wang W, Tao H, Zhao Y, Sun X, Tang J, Selomulya C, et al. Implantable and biodegradable macroporous iron oxide frameworks for efficient regeneration and repair of infracted heart. Theranostics. 2017; 7: 1966-75.
2. Besser RR, Ishahak M, Mayo V, Carbonero D, Claure I, Agarwal A. Engineered microenvironments for maturation of stem cell derived cardiac myocytes. Theranostics. 2018; 8: 124-40.
3. Choi YJ, Yi HG, Kim SW, Cho DW. 3D cell printed tissue analogues: a new platform for theranostics. Theranostics. 2017; 7: 3118-37.
4. Navaei A, Saini H, Christenson W, Sullivan RT, Ros R, Nikkhah M. Gold nanorod-incorporated gelatin-based conductive hydrogels for engineering cardiac tissue constructs. Acta Biomater. 2016; 41: 133-46.
5. Tao ZW, Mohamed M, Hogan M, Gutierrez L, Birla RK. Optimizing a spontaneously contracting heart tissue patch with rat neonatal cardiac cells on fibrin gel. J Tissue Eng Regen Med. 2017; 11: 153-63.
6. Ren J, Xu Q, Chen X, Li W, Guo K, Zhao Y, et al. Superaligned carbon nanotubes guide oriented cell growth and promote electrophysiological homogeneity for synthetic cardiac tissues. Adv Mater. 2017; 29: 1702713.
7. Spadaccio C, Nappi F, De Marco F, Sedati P, Taffon C, Nenna A, et al. Implantation of a poly-L-lactide GCSF-functionalized scaffold in a model of chronic myocardial infarction. J Cardiovasc Transl Res. 2017; 10: 47-65.
8. Hung GU, Ko KY, Lin CL, Yen RF, Kao CH. Impact of initial myocardial perfusion imaging versus invasive coronary angiography on outcomes in coronary artery disease: a nationwide cohort study. Eur J Nucl Med Mol Imaging. 2018; 45: 567-74.
9. Smits AM, Dronkers E, Goumans MJ. The epicardium as a source of multipotent adult cardiac progenitor cells: their origin, role and fate. Pharmacol Res. 2018; 127: 129-40.
10. Liu YL, Niu RC, Yang F, Yan Y, Liang SY, Sun YL, et al. Biological characteristics of human menstrual blood-derived endometrial stem cells. J Cell Mol Med. 2018; 22: 1627-39.
11. Bei Y, Das S, Rodosthenous RS, Holvoet P, Vanhaverbeke M, Monteiro MC, et al. Extracellular vesicles in cardiovascular theranostics. Theranostics. 2017; 7: 4168-82.
12. Gao L, Kupfer ME, Jung JP, Yang LB, Zhang P, Sie YD, et al. Myocardial tissue engineering with cells derived from human-induced pluripotent stem cells and a native-Like, high-resolution, 3-dimensionally printed scaffold. Circ Res. 2017; 120: 1318-25.
13. Martins AM, Eng G, Caridade SG, Mano JF, Reis RL, Vunjak-Novakovic G. Electrically conductive chitosan/carbon scaffolds for cardiac tissue engineering. Biomacromolecules. 2014; 15: 635-43.
14. Wu YB, Wang L, Guo BL, Ma PX. Interwoven aligned conductive nanofiber yarn/hydrogel composite scaffolds for engineered 3D cardiac anisotropy. ACS Nano. 2017; 11: 5646-59.
15. Prabhakaran MP, Kai D, Ghasemi-Mobarakeh L, Ramakrishna S. Electrospun biocomposite nanofibrous patch for cardiac tissue engineering. Biomed Mater. 2011; 6: 055001.
16. Wanjare M, Hou L, Nakayama KH, Kim JJ, Mezak NP, Abilez OJ, et al. Anisotropic microfibrous scaffolds enhance the organization and function of cardiomyocytes derived from induced pluripotent stem cells. Biomater Sci. 2017; 5: 1567-78.
17. Stoppel WL, Hu DJ, Domian IJ, Kaplan DL, Black LD. Anisotropic silk biomaterials containing cardiac extracellular matrix for cardiac tissue engineering. Biomed Mater. 2015; 10: 034105.
18. Kitsara M, Agbulut O, Kontziampasis D, Chen Y, Menasche P. Fibers for hearts: A critical review on electrospinning for cardiac tissue engineering. Acta Biomater. 2017; 48: 20-40.
19. Zhang YS, Arneri A, Bersini S, Shin SR, Zhu K, Goli-Malekabadi Z, et al. Bioprinting 3D microfibrous scaffolds for engineering endothelialized myocardium and heart-on-a-chip. Biomaterials. 2016; 110: 45-59.
20. Radisic M, Fast VG, Sharifov OF, Iyer RK, Park H, Vunjak-Novakovic G. Optical mapping of impulse propagation in engineered cardiac tissue. Tissue Eng Part A. 2009; 15: 851-60.
21. Dong R, Zhao X, Guo B, Ma PX. Self-healing conductive injectable hydrogels with antibacterial activity as cell delivery carrier for cardiac cell therapy. ACS Appl Mater Interfaces. 2016; 8: 17138-50.
22. Spearman BS, Hodge AJ, Porter JL, Hardy JG, Davis ZD, Xu T, et al. Conductive interpenetrating networks of polypyrrole and polycaprolactone encourage electrophysiological development of cardiac cells. Acta Biomater. 2015; 28: 109-20.
23. Cui Z, Ni NC, Wu J, Du GQ, He S, Yau TM, et al. Polypyrrole-chitosan conductive biomaterial synchronizes cardiomyocyte contraction and improves myocardial electrical impulse propagation. Theranostics. 2018; 8: 2752-64.
24. Sun M, Guo J, Hao H, Tong T, Wang K, Gao W. Tumour-homing chimeric polypeptide-conjugated polypyrrole nanoparticles for imaging-guided synergistic photothermal and chemical therapy of cancer. Theranostics. 2018; 8: 2634-45.
25. Guo B, Ma P. Conducting polymers for tissue engineering. Biomacromolecules. 2018; 19: 1764-82.
26. Zhao X, Li P, Guo B, Ma PX. Antibacterial and conductive injectable hydrogels based on quaternized chitosan-graft-polyaniline/oxidized dextran for tissue engineering. Acta Biomater. 2015; 26: 236-48.

27. Chuangchote S, Sagawa T, Yoshikawa S. Fabrication and optical properties of electrospun conductive polymer nanofibers from blended polymer solution. Jpn J Appl Phys. 2008; 47: 787-93.

28. Kai D, Prabhakaran MP, Jin G, Ramakrishna S. Polypyrrole-contained electrospun conductive nanofibrous membranes for cardiac tissue engineering. J Biomed Mater Res A. 2011; 99: 376-85.

29. Lee JY, Bashur CA, Goldstein AS, Schmidt CE. Polypyrrole-coated electrospun PLGA nanofibers for neural tissue applications. Biomaterials. 2009; 30: 4325-35.

30. Cikova E, Micusik M, Siskova A, Prochazka M, Fedorko P, Omastova M. Conducting electrospun polycaprolactone/polypyrrole fibers. Synthetic Met. 2018; 235: 80-8.

31. Wang LY, Jiang JZ, Hua WX, Darabi A, Song XP, Song C, et al. Mussel-inspired conductive cryogel as cardiac tissue patch to repair myocardial infarction by migration of conductive nanoparticles. Adv Funct Mater. 2016; 26: 4293-305.

32. Cowger TA, Tang W, Zhen Z, Hu K, Rink DE, Todd TJ, et al. Casein-coated Fe5C2 nanoparticles with superior r2 relaxivity for liver-specific magnetic resonance imaging. Theranostics. 2015; 5: 1225-32.

33. Tao W, Zeng X, Wu J, Zhu X, Yu X, Zhang X, et al. Polydopamine-based surface modification of novel nanoparticle-aptamer bioconjugates for in vivo breast cancer targeting and enhanced therapeutic effects. Theranostics. 2016; 6: 470-84.

34. Zhao H, Chao Y, Liu JJ, Huang J, Pan J, Guo WL, et al. Polydopamine coated single-walled carbon nanotubes as a versatile platform with radionuclide labeling for multimodal tumor imaging and therapy. Theranostics. 2016; 6: 1833-43.

35. Yaghoubi SS, Campbell DO, Radu CG, Czernin J. Positron emission tomography reporter genes and reporter probes: gene and cell therapy applications. Theranostics. 2012; 2: 374-91.

36. Wang ZY, Xing M, Ojo O. Mussel-inspired ultrathin film on oxidized Ti-6Al-4V surface for enhanced BMSC activities and antibacterial capability. RSC Adv. 2014; 4: 55790-9.

37. Jiang J, Wan W, Ge L, Bu S, Zhong W, Xing M. Mussel-inspired nanofibrous sheet for suture-less stomach incision surgery. Chem Commun. 2015; 51: 8695-8.

38. Zhao X, Dong R, Guo B, Ma PX. Dopamine-incorporated dual bioactive electroactive shape memory polyurethane elastomers with physiological shape recovery temperature, high stretchability, and enhanced C2C12 myogenic differentiation. ACS Appl Mater Interfaces. 2017; 9: 29595-611.

39. Ramanaviciene A, Kausaite A, Tautkus S, Ramanavicius A. Biocompatibility of polypyrrole particles: an in-vivo study in mice. J Pharm Pharmacol. 2007; 59: 311-5.

40. Vaitkuviene A, Kaseta V, Voronovic J, Ramanauskaite G, Biziuleviciene G, Ramanaviciene A, et al. Evaluation of cytotoxicity of polypyrrole nanoparticles synthesized by oxidative polymerization. J Hazard Mater. 2013; 250: 167-74.

41. Yang K, Xu H, Cheng L, Sun CY, Wang J, Liu Z. In vitro and in vivo near-infrared photothermal therapy of cancer using polypyrrole organic nanoparticles. Adv Mater. 2012; 24: 5586-92.

42. Kaur G, Adhikari R, Cass P, Bown M, Gunatillake P. Electrically conductive polymers and composites for biomedical applications. RSC Adv. 2015; 5: 37553-67.

43. Jang LK, Kim S, Seo J, Lee JY. Facile and controllable electrochemical fabrication of cell-adhesive polypyrrole electrodes using pyrrole-RGD peptides. Biofabrication. 2017; 9: 045007.

44. Wu Y, Wang L, Guo B, Shao Y, Ma PX. Electroactive biodegradable polyurethane significantly enhanced Schwann cells myelin gene expression and neurotrophin secretion for peripheral nerve tissue engineering. Biomaterials. 2016; 87: 18-31.

45. Tondera C, Hauser S, Kruger-Genge A, Jung F, Neffe AT, Lendlein A, et al. Gelatin-based hydrogel degradation and tissue interaction in vivo: insights from multimodal preclinical imaging in immunocompetent nude mice. Theranostics. 2016; 6: 2114-28.

46. Huang QQ, Wang FB, Yuan CH, He ZB, Rao L, Cai B, et al. Gelatin nanoparticle-coated silicon beads for density-selective capture and release of heterogeneous circulating tumor cells with high purity. Theranostics. 2018; 8: 1624-35.

47. Guerra AD, Yeung OWH, Qi X, Kao WJ, Man K. The anti-tumor effects of M1 macrophage-loaded poly (ethylene glycol) and gelatin-based hydrogels on hepatocellular carcinoma. Theranostics. 2017; 7: 3732-44.

48. Perikamana SKM, Lee J, Lee YB, Shin YM, Lee EJ, Mikos AG, et al. Materials from mussel-inspired chemistry for cell and tissue engineering applications. Biomacromolecules. 2015; 16: 2541-55.

49. Jensen L, Neri E, Bassaneze V, De Almeida Oliveira NC, Dariolli R, Turaca LT, et al. Integrated molecular, biochemical, and physiological assessment unravels key extraction method mediated influences on rat neonatal cardiomyocytes. J Cell Physiol. 2018; 233: 5420-30.

50. Shin SR, Jung SM, Zalabany M, Kim K, Zorlutuna P, Kim SB, et al. Carbon-nanotube-embedded hydrogel sheets for engineering cardiac constructs and bioactuators. ACS Nano. 2013; 7: 2369-80.

51. Shin H, Olsen BD, Khademhosseini A. The mechanical properties and cytotoxicity of cell-laden double-network hydrogels based on photocrosslinkable gelatin and gellan gum biomacromolecules. Biomaterials. 2012; 33: 3143-52.

52. Mihic A, Cui Z, Wu J, Vlacic G, Miyagi Y, Li SH, et al. A conductive polymer hydrogel supports cell electrical signaling and improves cardiac function after implantation into myocardial infarct. Circulation. 2015; 132: 772-84.

53. Sharma P, Abbasi C, Lazic S, Teng A, Wang D, Dubois N, et al. Evolutionarily conserved intercalated disc protein Tmem65 regulates cardiac conduction and connexin 43 function. Nat Commun. 2015; 6: 8391.

54. Zhang D, Shadrin I, Lam J, Xian H, Snodgrass H, Bursac N. Tissue-engineered cardiac patch for advanced functional maturation of human ESC-derived cardiomyocytes. Biomaterials. 2013; 34: 5813-20.

55. Cheng H, Cannell MB, Lederer WJ. Partial inhibition of Ca2+ current by methoxyverapamil (D600) reveals spatial nonuniformities in [Ca2+]i during excitation-contraction coupling in cardiac myocytes. Circ Res. 1995; 76: 236-41.

56. Koshy ST, Ferrante TC, Lewin SA, Mooney DJ. Injectable, porous, and cell-responsive gelatin cryogels. Biomaterials. 2014; 35: 2477-87.

57. Lee JW, Serna F, Nickels J, Schmidt CE. Carboxylic acid-functionalized conductive polypyrrole as a bioactive platform for cell adhesion. Biomacromolecules. 2006; 7: 1692-5.

58. Shin HY, Jung JY, Kim SW, Lee WK. XPS analysis on chemical properties of calcium phosphate thin films and osteoblastic HOS cell responses. J Ind Eng Chem. 2006; 12: 476-83.

59. Pham QP, Sharma U, Mikos AG. Electrospinning of polymeric nanofibers for tissue engineering applications: A review. Tissue Eng. 2006; 12: 1197-211.

60. Kwon IK, Kidoaki S, Matsuda T. Electrospun nano- to microfiber fabrics made of biodegradable copolyesters: structural characteristics, mechanical properties and cell adhesion potential. Biomaterials. 2005; 26: 3929-39.

61. You J, Rafat M, Ye G, Auguste D. Nanoengineering the heart: conductive scaffolds enhance connexin 43 expression. Nano Lett. 2011; 11: 3643-8.

62. Kim DH, Kim P, Song I, Cha JM, Lee SH, Kim B, et al. Guided three-dimensional growth of functional cardiomyocytes on polyethylene glycol nanostructures. Langmuir. 2006; 22: 5419-26.

63. Wang L, Wu YB, Hu TL, Guo BL, Ma PX. Electrospun conductive nanofibrous scaffolds for engineering cardiac tissue and 3D bioactuators. Acta Biomater. 2017; 59: 68-81.

64. Baei P, Jalili-Firoozinezhad S, Rajabi-Zeleti S, Tafazzoli-Shadpour M, Baharvand H, Aghdami N. Electrically conductive gold nanoparticle-chitosan thermosensitive hydrogels for cardiac tissue engineering. Mater Sci Eng C Mater Biol Appl. 2016; 63: 131-41.

65. Cochain C, Channon KM, Silvestre JS. Angiogenesis in the infarcted myocardium. Antioxid Redox Signal. 2013; 18: 1100-13.

66. Pal K, Banthia AK, Majumdar DK. Preparation and characterization of polyvinyl alcohol-gelatin hydrogel membranes for biomedical applications. AAPS PharmSciTech. 2007; 8: 21.

67. Zhou J, Chen J, Sun HY, Qiu XZ, Mou YC, Liu ZQ, et al. Engineering the heart: Evaluation of conductive nanomaterials for improving implant integration and cardiac function. Sci Rep. 2014; 4: 3733.